ACS OMEGA

Open Access

http://pubs.acs.org/journal/acsodf

Article

Exploring the Experimental and Theoretical Studies and Inhibition Mechanism of Passiflora Incarnata Extract as a Novel Green Inhibitor for API 5CT N80 in an Aggressive Environment

Abeer Y. H. Alamry, Nora S. Al-Subaie, Wafa S. Alshahrani, Mai M. A. H. Shanab, and Mariem M. Motawea*

Cite This: *ACS Omega* 2024, 9, 44697−44713

Read Online

ACCESS | Metrics & More | Article Recommendations

ABSTRACT: Corrosion is a crucial problem worldwide that heavily affects natural and industrial environments and can cause machinery breakdown and deterioration of construction assemblies, thus threatening the lives of humans and accelerating the consumption of natural metal reservoirs. In this study, we deployed passiflora incarnata extract (PIE) as an eco-friendly green inhibitor to prevent API 5CT N80 (CS-N80) corrosion in 1 M HCl. The chromatograms of the gas chromatography−mass spectroscopy analysis of PIE have identified 25 compounds. The weight loss method reveals that 150 ppm of the extract offers 90.4% inhibition efficiency (IE) to CS-N80 immersed in 1 M HCl solution at 25 °C. However, at higher temperatures (45 °C), % IE increases and reaches 92.1%. The electrochemical characterization of the adsorbed layer on CS-N80 was tested by utilizing electrochemical methods (electrochemical impedance spectroscopy and polarization) in 1 M HCl. Polarization diagrams displayed that PIE is a mixed-type inhibitor that retards CS-N80 corrosion. Temkin adsorption isotherm is the best fit for adsorbed PIE on the CS-N80 surface. IE was improved by raising the temperature (chemical adsorption). Examining the morphology of CS-N80 sheets through scanning electron microscopy, energy-dispersive X-ray, X-ray photoelectron spectroscopy, and Fourier transform infrared analysis furnishes valuable insights into their surface characteristics. The results of a quantum chemical computation show that the three PIE components have strong anticorrosion properties. According to findings from molecular dynamics simulations, the three PIE components can have a high binding energy and can be adsorbed in a parallel manner at the Fe(110) surface. All tests have shown that the PIE composite conversion adsorbed with a self-healing property and lower corrosion current density was precipitated on the steel surface.

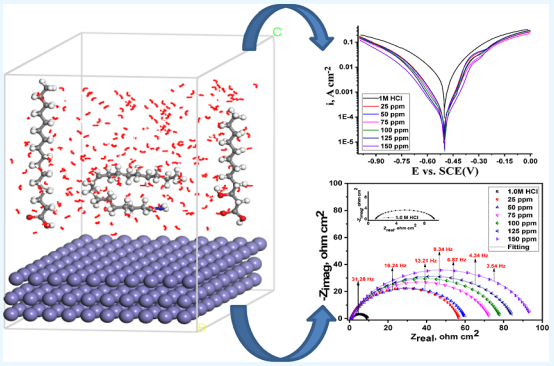

1. INTRODUCTION

Corrosion studies are a big deal to maintain metal resources, benefit from rare and expensive metals to the highest extent, and broaden the usage of novel high-strength metal alloys. There is a daily economic loss of metal which can be classified into direct loss and indirect loss.[1] One of the most effective methods for resisting corrosion in acidic environments is the use of inhibitors. Among the various materials that can corrode, carbon steel is often basically an alloy of steel that accommodates 0.12−2% carbon; the more carbon present inside the steel, the tougher and more powerful it becomes. It can also become less ductile, which means the strength can be decremented when distorted and is not as docile.[2] Many manufacturers view CS as the most usable material due to its exceptional mechanical qualities and extremely low cost. In 2020, a production of 1864.0 million tonnes was witnessed; however, 20% of that amount was likely to be used for the repair of corroded equipment or infrastructure.[3] Acidic solutions are employed in several processes, such as chemical petrochemical operations, metal picking to reduce scale, and the manufacture of components for rocket tools.[4] The equipment is cleaned using mineral acids, but these acids lead to rusting. As a result, inhibitors are widely employed to lessen acids' tendency to corrode.

On the other hand, the selection of any inhibitor is greatly impacted by its cost, effectiveness at suppressing the corrosion of the metal, and adverse impacts on the environment.[5] Inhibitors made from plant extracts are distinguished by their availability, affordability, and lack of adverse environmental impacts.[6] The utilization of inhibitors that are created by plants can make a

Received: August 15, 2024
Revised: October 7, 2024
Accepted: October 11, 2024
Published: October 21, 2024

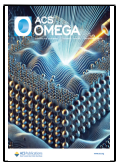

significant upgrade to both corrosion resistance and inhibition efficiency (IE). They are eco-friendly as they do not harm both people and the environment, are inexpensive to execute, and can be used in various situations and with various types of materials. Researchers have detected many phytochemicals included in plants that can withstand rust formation.[7]

The primary benefits of utilizing plant extracts as corrosion inhibitors are cost-effectiveness and safety from an ecological standpoint.[8] Recently, a variety of extracts have been used to effectively mitigate the corrosion of CS metals under acidic conditions, including *Viscum album*,[9] *Clinopodium acinos*,[10] *Nerium oleander*,[11] *Pulicaria undulate*,[12] *Aizoon canariense*,[13] *Aconitum carmichaelii* Debx,[14] *Vernonia amygdalina* Leaf,[15] and *Erica arborea*.[16] It is well known that the presence of a complex of organic chemicals, including flavonoids, polyphenols, nitrogen, alkaloid bases,[17,18] proteins, amino acids,[19] and sugars, together with potential hydrolysis molecules in their structure, is responsible for the inhibition action of extracts.[20] These naturally occurring organic compounds typically have triple and double bonds in assemblies, or conjugated or aromatic rings, in addition to their polar utility with donor atoms like O, S, N, and C, assist in extracts' molecule adsorption onto the metal surfaces, creating a protective layer that inhibits their corrosion, all of which help in the adsorption of these compounds on the metal surface and thus protect it from corrosion.[21]

Plant extracts have been widely studied as inhibitors due to their low cost, abundant availability, and biodegradability. This research tries to investigate the effectiveness of passiflora incarnata extract (PIE) in inhibiting CS-N80 corrosion in hydrochloric acid solutions. This will be achieved through chemical and electrochemical studies, as well as surface analysis using scanning electron microscopy (SEM), energy-dispersive X-ray, X-ray photoelectron spectroscopy (XPS), and Fourier transform infrared (FT-IR) examinations to verify the extract's adsorption.

2. EXPERIMENTAL MEASUREMENTS

2.1. Preparations of Metals. The steel used was an N80-grade C steel in accordance with API SPEC 5CT.[22] API 5CT N80 specimen analysis indicated the presence of the following components: 0.34% C, 1.45% Mn, 0.02% P, 0.2% Si, 0.015% S, 0.15% Cr, and balance Fe. For weight loss (WL) tests, the API 5CT N80 samples' geometric scale was 20 × 20 × 2 mm, while for electrochemical measurements, the exposed surface area was 10 × 10 mm; additionally, samples were abraded before the assessment (with varying emery papers' grades, 320−2500) until a mirror finish appeared.

2.2. Investigational Solution Preparation. The corrosive acidic solution (1 molar HCl) was formed using a 37% HCl analytical grade reagent and bidistilled water. This medium was subsequently utilized to prepare five various molar concentrations (of each inhibitor: 25, 50, 75, 100, 125, and 150 ppm).

2.2.1. Preparation of PIE. The PIE plant components were collected and manually washed with distilled water to remove dust or other residues that were detached. After being shaded at room temperature and ground into a fine powder using an electronic mill, 20 g of the powder was placed in a 500 mL measuring flask and dissolved in bidistilled water, and the flask was left on a hot plate. After allowing it to cool at room temperature, the filtrate (10 mL) was taken with 5 mL of ethanol and placed in a condensate-collecting flask of a rotary evaporator to quantify the amount of dissolved material in the plant extract solution. At last, the concentrate was gathered, weighed, and stored in tightly sealed bottles for gas chromatography−mass spectroscopy (GC−MS). By adding 1000 mL of bidistilled water to 1 g of the extract, a stock solution of 1000 ppm was created. The concentration of the extract that was utilized ranged from 25 to 150 ppm and was made by diluting PIE with bidistilled water.

2.2.2. Chemical Constituents of PIE by Using GC−MS. A study using GC−MS was performed at the Egyptian National Centre. Accomplished at a voltage of 70 eV (m/z 50−550, source at 230 °C, and quadruple at 150 °C), GC analytes were identified using an HP model 6890 GC interfaced to an HP 5791A mass selective detector.

2.3. WL Tests. For corrosion research, WL is perhaps the method used most frequently. This method is perfect for beginners because it is simple to use and does not require a lot of equipment. Sized at 2 cm × 2 cm × 0.2 cm, the CS-N80 specimens underwent mechanical polishing and abrading with emery papers ranging in grade from 250 to 1200. Following this, they were cleaned with bidistilled water, brushed with acetone, and then dried using filter papers, according to the standard way. At temperatures ranging from 25 to 45 °C, the specimens, after weighing, were submerged in 100 mL beakers containing different concentrations of PIE along with 1 M HCl. After varying times (30−60−90−120−150 to 180 min), the CS-N80 specimens were removed from the solution, washed, dried, and weighed once more. The assessed WL can be employed to determine the CS-N80′ surface area that is covered (θ), and the effectiveness of inhibition (% IE) can be calculated using the following equation[23]

$$\%\ \mathrm{IE} = \theta \times 100 = \left(1 - \frac{\Delta W_{\mathrm{inh}}}{\Delta W_{\mathrm{free}}}\right) \times 100 \tag{1}$$

where the WL (mg) with and without PIE is represented as ΔW_{inh} and ΔW_{free}, respectively. The corrosion rate (CR) of the metal sample was calculated using the following equation

$$\mathrm{CR} = \frac{\Delta W}{AT} \tag{2}$$

where A (cm^2) is the specimen surface area, t (min) is the time, and ΔW (mg) is the weight reduction.

2.4. Electrochemical Tests. The Gamry device cell (PCI4/750) Potentiostat/Galvanostat/ZRA comprises three electrodes: a SCE serving as the reference, a platinum wire serving as the counter electrode, and CS-N80 serving as the working electrode.[24] A square sample of the working electrode measuring 1 × 1 cm was used. Just as in the WL approach, the electrode surface has been handled. Every electrochemical measurement was run at 25 °C. The testing was started after allowing the CS to stabilize for 30 min prior to measurement.

2.4.1. Potentiodynamic Polarization. Tafel curves were developed using potentiodynamic polarization (PP) analysis, applying potentials between −500 and 500 V versus OCP with 0.1 mV s^{-1} scan rate. The values of corrosion potential (E_{corr}) and corrosion current density (i_{corr}) were computed by the Tafel areas' cathodic and anodic line extrapolation. The inhibition percentage is calculated from the equation. The values of θ and % IE from the PP test were calculated as follows[25]

$$\%\ \mathrm{IE} = \theta \times 100 = \left[1 - \frac{i_{\mathrm{corr(inh)}}}{i_{\mathrm{corr(free)}}}\right] \times 100 \tag{3}$$

https://doi.org/10.1021/acsomega.4c07543
ACS Omega 2024, 9, 44697−44713

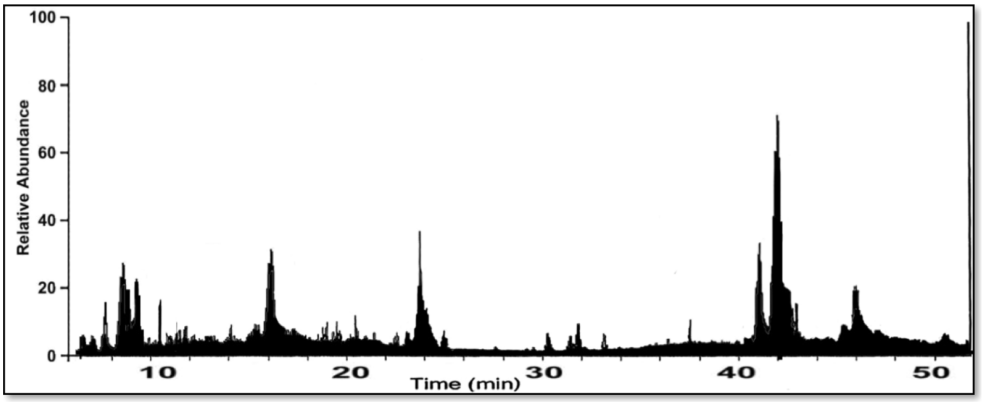

Figure 1. GC−MS of PIE.

Table 1. Recognized Phytochemicals Found in PIE

no	chemical constituent	percent peak area
1	isoschaftoside	0.361
2	4*H*-pyran-4-one, 2,3-dihydro-3,5-dihydroxy-6-methyl-	4.988
3	1-pentanol, 2-methyl-, acetate	0.524
4	8-(*β*-D-glucopyranosyl)-4′,5,7-trihydroxyflavone	0.524
5	4-cyclopropylcarbonyloxytridecane	0.604
6	5-cyclopropylcarbonyloxypentadecane	0.857
7	isoorientin 2″-*O*-glucopyranoside	0.135
8	9-tetradecen-1-ol, acetate, (E)	0.566
9	*trans*-2-undecenoic acid	0.324
10	dodecanoic acid, 3-hydroxy	17.78
11	D-mannose	0.224
12	7-methyl-Z-tetradecen-1-ol acetate	0.478
13	l-gala-*l*-ido-octose	0.314
14	*n*-hexadecanoic acid; (palmitic acid)	24.98
15	phytol	0.987
16	9-hexadecyn-1-ol	0.867
17	cis,cis,*cis*-7,10,13-hexadecatrienal	1.879
18	octadecanoic acid	1.111
19	9-octadecenamide, (Z)-; (oleamide)	34.66
20	9,10-secocholesta-5,7,10(19)-triene-3,24,25-triol, (3*β*,5Z,7E)	0.987
21	ethyl 9-hexadecenoate	1.278
22	pregnane-3,11,20,21-tetrol, cyclic 20,21-(butyl boronate), (3*α*,5*β*,11*β*,20R)	1.578
23	vitamin E	1.897
24	*β*-sitosterol	0.987
25	stigmasterol	1.109

where $i_{corr(inh)}$ denotes the corrosion current density in the inhibitor solution and $i_{corr(free)}$ denotes the corrosion current density in the blank solution.

The electrochemical impedance spectroscopy (EIS) tests were carried out at the OCP using AC signals with an amplitude of 10 mV, in the frequency range of 1×10^5 to 0.1 Hz. Below is the equation used to determine the values of θ and % IE from EIS experiments[26]

$$\% \text{ IE} = \theta \times 100 = \left[1 - \frac{R_{p(free)}}{R_{p(inh)}}\right] \times 100 \quad (4)$$

where $R_{p(free)}$ represents the charge-transfer resistance in the blank solution and $R_{p(inh)}$ represents the charge-transfer resistance in the inhibited solution.

2.5. Surface Morphology. *2.5.1. SEM Analysis.* SEM tests were performed on a 2 × 2 cm CS-N80 surface before and after immersing it in 1 M HCl for 24 h without PIE and with 150 ppm of PIE. Using a JEOL JSM-6510 microscope, the morphology of the CS-N80 surface under protection and without it was examined.

2.5.2. Atomic Force Microscopy Analysis. Using the atomic force spectroscopy technique atomic force microscopy (AFM) (Nanosurf C3000 Software, version, 3.5.0.31), the morphological properties of the CS-N80 metal surface were studied. AFM inspections were performed for the CS-N80 surface prior to and after submerging in 1 M HCl for 1 day without and with 150 ppm of PIE. AFM was carried out in contact mode using a silicon nitride probe (MLCT model; Bruker).

2.5.3. XPS Examination. XPS (AXIX Ultra DLD, Kratos, UK): This method depends on the atomic energy spectra of the inhibited molecules, which give a strong detection of the structure of the inhibitor adsorbed on a metal surface in addition to the detection of the inhibitor−metal surface reaction type.

2.5.4. FT-IR Analysis. To learn more about the inhibitor's functional groups both before and after it is adsorbed on the

https://doi.org/10.1021/acsomega.4c07543
ACS Omega 2024, 9, 44697−44713

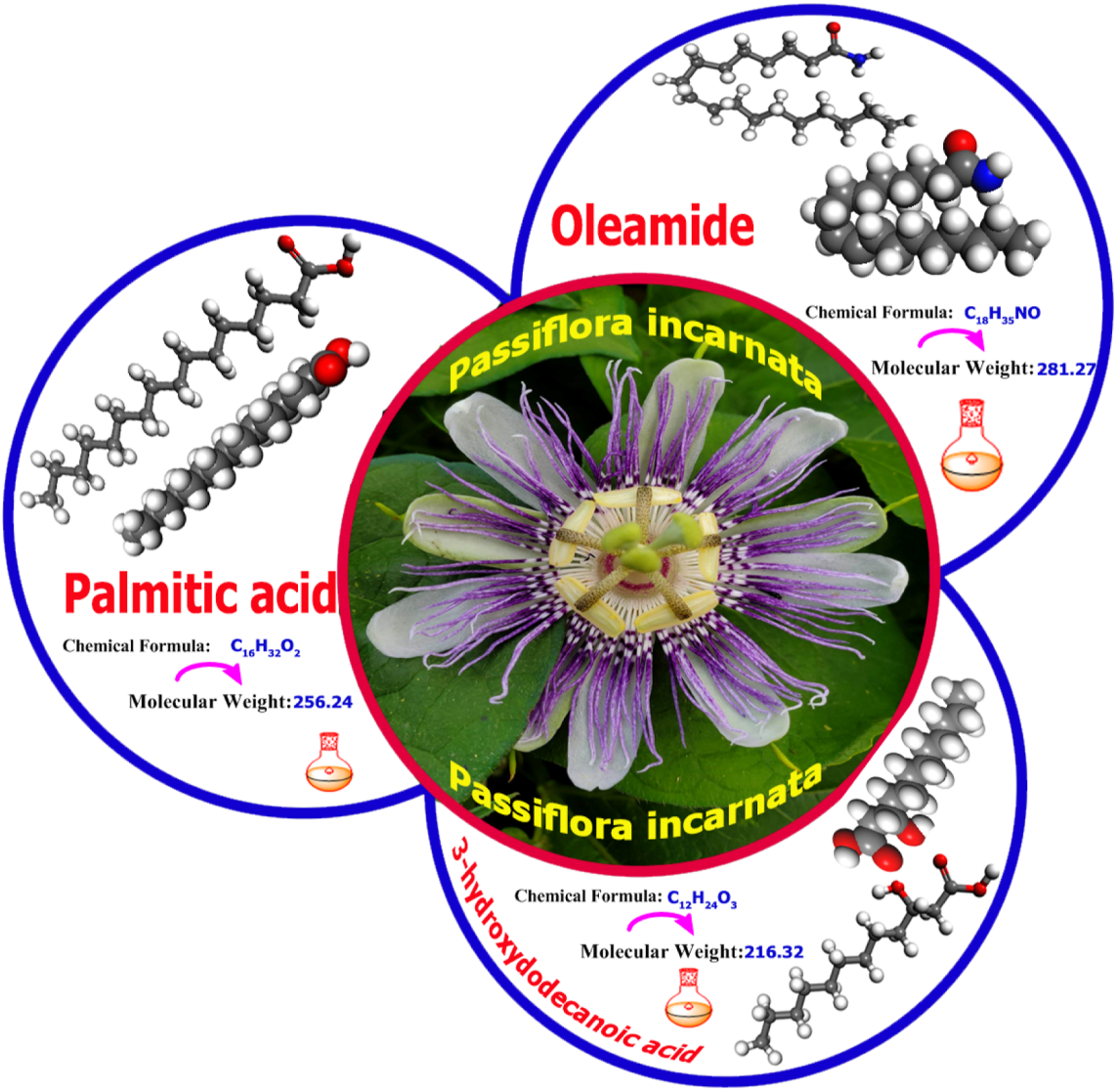

Figure 2. Main components of PIE.

metal, FT-IR analyses were performed to identify the structure of the spectrum inhibitor that produces peaks with specific values. After the 2 cm × 2 cm CS-N80 specimen was prepared according to the WL procedure, it was immersed for 24 h in 1 M HCl containing 150 ppm of PIE and then investigated directly using FT-IR spectra attenuated total reflectance mode and an iS 10 FTIR-Spectrometer from Thermo Fisher Scientific (USA).

2.6. Density Functional Theory and Monte Carlo Theoretical Calculations. *2.6.1. Quantum Chemical Calculation.* The quantum chemical computations were performed using Gaussian 09 software, Revision A02.[40] To identify which inhibitor had the lowest energy, the inhibitors in the study were first examined using molecular mechanics optimization of the conformers.[27] The calculations began without any geometry restrictions and were performed for the neutral species of the molecules under investigation until complete geometry optimization was attained in the ground state. For every optimized structure, the calculated vibrational modes showed no imaginary frequency. The density functional theory (DFT) approach was used without symmetry constraints and at the 6-31G++(d,p) basis set level. The Becke three-parameter hybrid B3[28] with the L−Y−P (Lee−Yang−Parr) correction functional (B3LYP) was used for all geometry calculations using Gaussian 09. An alternative to Hartree−Fock calculations used in some cases is DFT, which treats both exchange and correlation energies, albeit approximately. An alternative to Hartree−Fock calculations used in some cases is DFT, which treats both exchange and correlation energies, albeit approximately.[29] Other significant quantum parameters were calculated by using the obtained quantum chemical parameters. The highest occupied molecular orbital (HOMO) and lowest unoccupied molecular orbital (LUMO) both have equivalent importance on the adsorption onto the metallic surface through the electro-donation or electro-acceptation mechanism.

2.6.2. Monte Carlo Simulations. MC stimulation was applied on the three major organic compound extracts from PIE in an aqueous solution and was functioned using DMol3 and adsorption locator modulation through material studio v.7.0 (by Accelrys Inc. USA). In addition to using global orbital cutoffs and fine convergence, water was established as a solvent to influence the treatment using the COSMO controls. Through the COSMO control, the effect of the solvent (aqueous phase) was incorporated into the DMol3 calculations. The effect of their inhibitory trail is evaluated by simulating the adsorption of

https://doi.org/10.1021/acsomega.4c07543
ACS Omega 2024, 9, 44697−44713

PIE molecules on the Fe (1 1 0) crystal using an adsorption locator module. The Fe (1 1 0) crystal and the inhibitor interact under periodic boundary conditions, constructed in the stimulation box (30.27 Å × 30.27 Å × 52.18 Å). Applying the Monte Carlo (MC) search in a test box with three molecules of inhibitors and a simulation-corrosive species, the simulation analysis was performed by assigning the high-quality force field known as COMPASS to three major organic compound extracts from PIE.[30]

3. RESULTS AND DISCUSSION

3.1. GC−MS Analysis of PIE. Figure 1 displays the GC−MS chromatograms of PIE. Table 1 shows the relative quantities (% peak area) of each of the 25 chemicals. 9-Octadecenamide, (*Z*)-; oleamide (34.66%); *n*-hexadecanoic acid; palmitic acid (24.98%); and 3-hydroxydodecanoic acid (17.78%) are the main constituents with higher percent peak area recognized. The molecular weights, structures, and formulas of oleamide, palmitic acid, and 3-hydroxydodecanoic acid are shown in Figure 2.

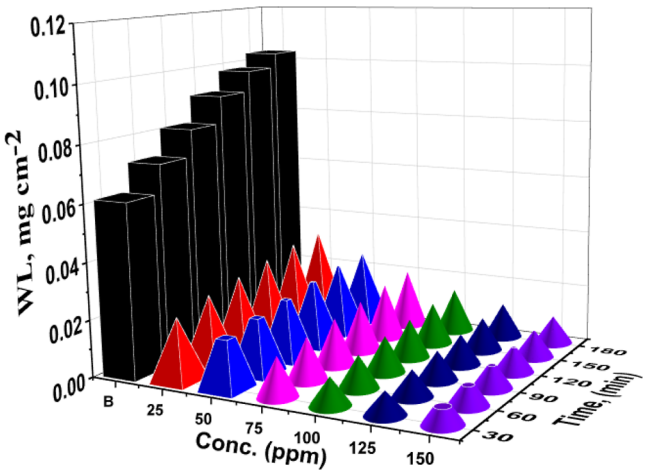

Figure 3. Time−WL graph of CS-N80 in a corrosive medium attendance and lack of various doses of various PIE at 298 K.

3.2. Weight Loss. At various times and temperatures (25−45 °C), the WL of CS-N80 in 1 M HCl was measured, both lacking and in varying PIE doses. The effect of adding varying amounts (25−150 ppm) of PIE on CS corrosion in a 1 M HCl solution was assessed by utilizing the WL method. The relationship between the impacts of various concentrations of PIE on CS-N80, WL vs time at 25 °C is depicted in Figure 3. It is evident that the WL of CS-N80 in the presence of PIE was significantly lower than that obtained in the blank solution. As the extract concentration grows, the layer created by the extract molecules adsorbed on the metal surface causes the WL to drop. This layer protects the metal's corrosive sites and keeps the metal from corroding in the corrosive environment, meaning that the higher quantity of PIE led to a higher % IE.

3.2.1. Effect of Temperature. One of the key tests to determine an inhibitor's effectiveness in preventing the corrosion of CS-N80 metal is WL testing. Through the use of WL tests, the impact of different temperatures (25, 30, 35, 40, and 45 °C) on the corrosion of CS-N80 in 1 M HCl in the presence and absence of various doses of PIE was investigated. Table 2 displays the estimates of CR and % IE derived from the WL tests for altered doses of PIE in 1 M HCl solution at altered temperatures in a time period of 2 h (120 min). The findings show that a rise in PIE doses leads to a reduction in CR value and an increase in % IE. This is a result of the extract's increasing degree of adsorption and subsequent covering of the CS surface as the extract concentration increases. The increase in % IE with

Table 2. WL Results for CS-N80 in 1 M HCl for Multiple Doses of PIE at Various Temperatures after 120 min

temp., °C	extract conc. (ppm)	k_{corr} (mg/cm² min)	θ	% IE
25	blank	0.0905 ± 0.0015		
	25	0.0295 ± 0.0018	67.4	0.674
	50	0.0228 ± 0.0020	74.8	0.748
	75	0.0180 ± 0.0022	80.1	0.801
	100	0.0137 ± 0.0021	84.9	0.849
	125	0.0108 ± 0.0015	88.1	0.881
	150	0.0087 ± 0.0017	90.4	0.904
30	blank	0.1158 ± 0.0019		
	25	0.0364 ± 0.0022	68.6	0.686
	50	0.0287 ± 0.0011	75.0	0.752
	75	0.0221 ± 0.0017	80.9	0.809
	100	0.0169 ± 0.0014	85.4	0.854
	125	0.0135 ± 0.0012	88.3	0.883
	150	0.0107 ± 0.0011	90.8	0.908
35	blank	0.1522 ± 0.0012		
	25	0.0460 ± 0.0017	69.8	0.698
	50	0.0364 ± 0.0016	76	0.761
	75	0.0286 ± 0.0014	81.2	0.812
	100	0.0216 ± 0.0022	85.8	0.858
	125	0.0174 ± 0.0025	88.6	0.886
	150	0.0139 ± 0.0017	90.9	0.909
40	blank	0.1601 ± 0.0011		
	25	0.0458 ± 0.0013	71.4	0.714
	50	0.0365 ± 0.0017	77.1	0.772
	75	0.0290 ± 0.0014	81.9	0.819
	100	0.0226 ± 0.0021	85.9	0.859
	125	0.0170 ± 0.0022	89.4	0.894
	150	0.0134 ± 0.0014	91.6	0.916
45	blank	0.2219 ± 0.0012		
	25	0.0601 ± 0.0011	72.9	0.729
	50	0.0479 ± 0.0017	78.4	0.784
	75	0.0388 ± 0.0021	82.5	0.825
	100	0.0295 ± 0.0022	86.7	0.867
	125	0.0220 ± 0.0020	90.1	0.901
	150	0.0175 ± 0.0011	92.1	0.921

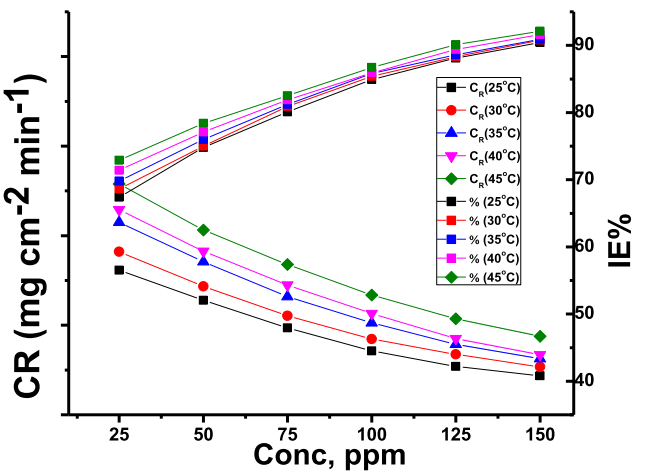

Figure 4. Impact of adding various PIE concentrations on % IE and CR.

https://doi.org/10.1021/acsomega.4c07543
ACS Omega 2024, 9, 44697−44713

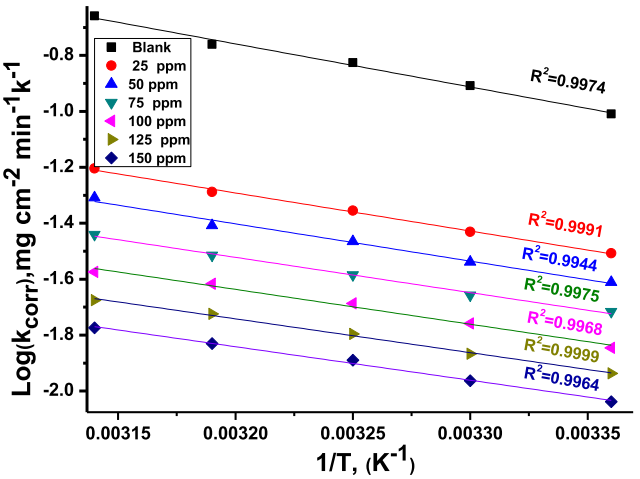

Figure 5. $1/T$ vs log k_{corr} for CS-N80 in the HCl solution with and without PIE at altered concentrations.

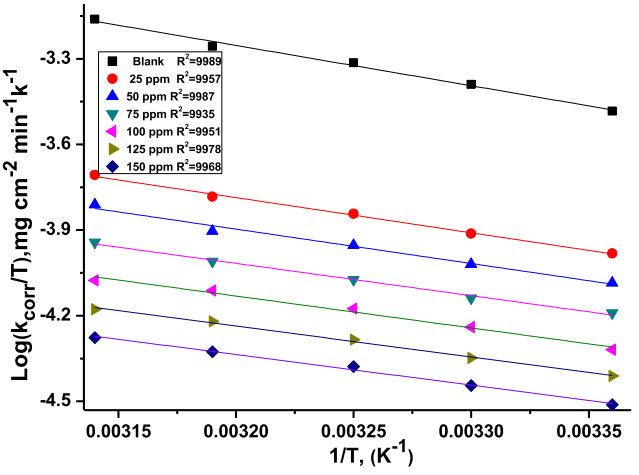

Figure 6. Plotting log k_{corr}/T against $1/T$ for CS-N80 in 1 M HCl with and without PIE at various concentrations.

Table 3. E_a*, ΔH*, and ΔS* for CS-N80 in 1M HCl at Various Doses and without PIE

Conc. ppm	E_a* kJ mol^{-1}	ΔH* kJ mol^{-1}	$-\Delta S$* J mol^{-1}K^{-1}
blank	29.4 ± 0.2319	27.1 ± 0.1478	173 ± 0.2022
25	26.1 ± 0.2004	23.5 ± 0.1745	194 ± 0.2124
50	25.5 ± 0.2105	23.1 ± 0.1547	198 ± 0.1145
75	24.1 ± 0.1754	21.6 ± 0.1245	205 ± 0.1247
100	23.8 ± 0.1475	21.3 ± 0.1412	208 ± 0.2017
125	23.1 ± 0.1125	20.6 ± 0.1954	212 ± 0.1124
150	22.9 ± 0.1247	20.4 ± 0.1214	214 ± 0.1324

increasing temperature shows that the extract may be chemisorbed on the CS-N80 surface. Increasing the temperature leads to an increase in the adsorption of inhibitor molecules on the alloy surface accompanied by charge transfer to form chemical bonds by sharing electrons with the Fe atoms on the surface, resulting in an increase in electron densities at the adsorption centers of the molecules, and this leads to the accumulation of a protective layer on the surface of the metal (Figure 4).[31]

WL tests at various temperatures with and without PIE can be used to calculate the energy (E_a*) of activation, as well as additional thermodynamic activation factors. The results could

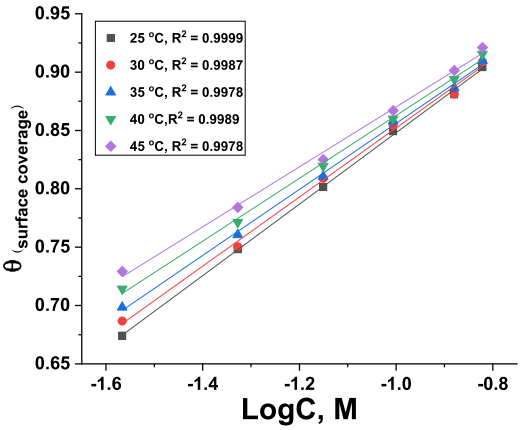

Figure 7. θ plot against C for CS-N80 dissolution with PIE at various temperatures.

be used to know the inhibitory mechanism. Using the Arrhenius equation, it was possible to estimate (E_a*) for CS-N80 corrosion in the blank and inhibited HCl solutions as follows[32]

$$\text{Log CR} = \log A - E_a^*/2.303RT \quad (5)$$

where A is the pre-exponential multiplier. As presented in Figure 5, the log CR against $1/T$ graphs with and without PIE at altered doses produced straight lines with slopes from which the E_a* values were obtained.[33] The following transition-state equation was utilized to calculate the entropy (ΔS*) and enthalpy (ΔH*) of activation for the corrosion of CS-N80.[34]

$$\text{Log}(\text{CR}/T) = [\log(R/Nh) + \Delta S_a^*/2.303R] - \Delta H_a^*/2.303RT) \quad (6)$$

where h is Planck's constant. Plots of $(1/T)$ versus $\log(\text{CR}/T)$ produced straight lines (Figure 6), and from their slopes and intercepts, the values of ΔH* and ΔS* were obtained, respectively. Table 3 contains the computed values for E_a*, ΔH*, and ΔS*, both with and without PIE present. The data in Table 3 indicate that the activation energy values are lower when the extract is present than it is absent. The decrease in E_a* indicates that the extract molecules are chemically adsorbed onto the metal surface.[35] The positive sign of ΔH* indicates that PIE molecules are adsorbed endothermically on the CS-N80 surface. The decreasing values of ΔH* in the PIE-containing solutions relative to the blank solutions show that the corrosion reaction energy barrier is decreasing. The resulting mean alteration among Ea* and ΔH* is about 2.6 kJ mol^{-1}, which is the same as the value of RT, which is 2.63 kJ/mol.[36] It is implied that disorder occurs during the transition from the reactant to the activated complex by the negative values of ΔS*, which shows that the activated complex inside the rate-determining step implies an association rather than a dissociation phase.

3.2.2. Adsorption Study. In order to study the metal surface coverage with PIE, the corrosion mechanism, numerous adsorption isotherms have been used. The suitable result is that of the Temkin adsorption isotherm.[37] According to the Temkin equation, the relationship between the PIE concentration (C) and the area of the CS-N80 surface covered by PIE (θ) is as follows

$$a\theta = \ln K_{ads}C \quad (7)$$

where K_{ads} stands for the equilibrium constant for adsorption and C_{inh} is the concentration by molarity of the tested PIE

https://doi.org/10.1021/acsomega.4c07543
ACS Omega 2024, 9, 44697−44713

Table 4. Parameters for PIE on CS-N80 Surface after 120 min of Immersion at Various Temperatures

temp. °C	a	log K_{ads}	$-\Delta G_{ads}^{\circ}$ kJ mol^{-1}	ΔH_{ads}° kJ mol^{-1}	ΔS_{ads}° J mol^{-1} K^{-1}
25	7.44	3.73842	31.2 ± 0.1273	59.1 ± 0.1653	105.1 ± 0.1214
30	7.77	3.87817	32.6 ± 0.1475		107.8 ± 0.2150
35	8.13	4.02552	34.1 ± 0.1758		110.6 ± 0.2014
40	8.55	4.20417	35.6 ± 0.1124		114.1 ± 0.1711
45	8.96	4.38629	37.3 ± 0.1987		117.5 ± 0.1624

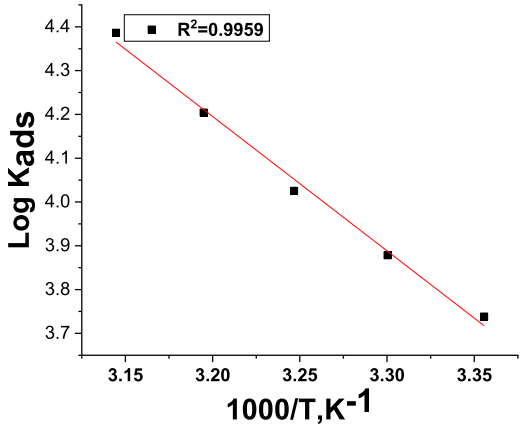

Figure 8. Log K_{ads} vs 1000/T graph for CS-N80 in 1 M HCl with PIE.

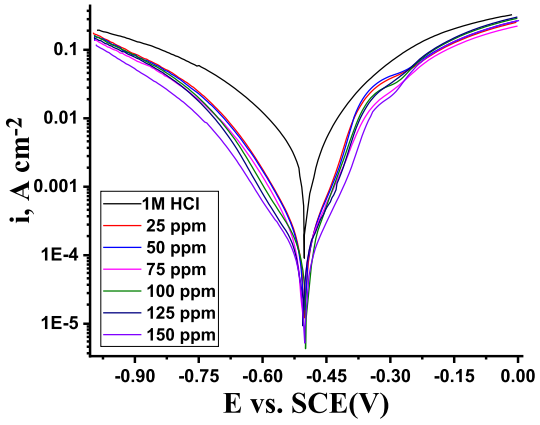

Figure 9. Displaying Tafel curves for the CS-N80 electrode in 1 M HCl with and without different altered doses of PIE at 298 K.

inhibitor. Figure 7 displays a graph of the Temkin isotherm at various temperatures. Following is the equation applied to attain the free energy of adsorption (ΔG_{ads}°)[38]

$$K_{ads} = (1/55.5)\exp(-\Delta G_{ads}^{\circ}/RT) \quad (8)$$

where 55.5 is the concentration of water, in mol/L, at the metal/solution interface. Table 4 contains the calculated values of K_{ads} and ΔG_{ads}°. The negative readings of ΔG_{ads}° designate that PIE

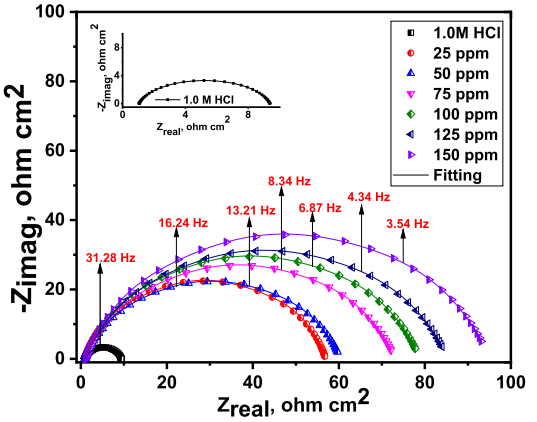

Figure 10. Nyquist diagrams for CS-N80 in 1 M HCl without and with multiple doses of PIE at 298 K.

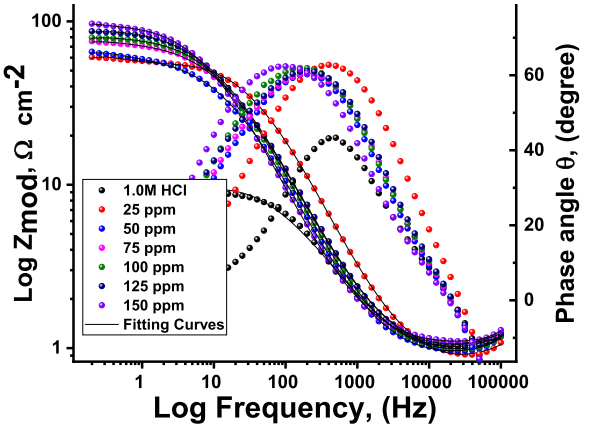

Figure 11. Bode plots with PIE and in varying PIE doses for CS-N80 in 1 M HCl at 25 °C.

is adsorbed spontaneously, and the adsorbed film on the CS-N80 surface is stable. Regarding the ΔG_{ads}° data, values close to −20 kJ mol^{-1} indicate physical adsorption, whereas values greater than −40 kJ mol^{-1} indicate chemisorption.[39] The values for ΔG_{ads}° that were found, which range from −31.2 to −37.3 kJ mol^{-1}, indicate that PIE molecules and the CS-N80 surface interact with mixed adsorption, mainly chemical. The following

Table 5. PP Parameters for the Corrosion of CS-N80 at 298 K without and with Multiple Doses of PIE

conc., ppm	I_{corr}, μA cm^{-2}	$-E_{corr}$, E vs SCE/V	$-\beta_a$, mV·dec^{-1}	β_c, mV·dec^{-1}	CR mm/yr	θ	% IE
blank	1168 ± 0.2102	502 ± 0.1174	101	157	220		
25	167 ± 0.2014	501 ± 0.1245	88	148	78	0.857	85.7
50	149 ± 0.1124	504 ± 0.1325	87	135	73	0.872	87.2
75	132 ± 0.1745	507 ± 0.1741	94	138	65	0.887	88.7
100	124 ± 0.1425	498 ± 0.1621	79	131	65	0.894	89.4
125	117 ± 0.1244	503 ± 0.1219	90	160	61	0.900	90.0
150	101 ± 0.1411	508 ± 0.1547	97	147	52	0.914	91.4

https://doi.org/10.1021/acsomega.4c07543
ACS Omega 2024, 9, 44697−44713

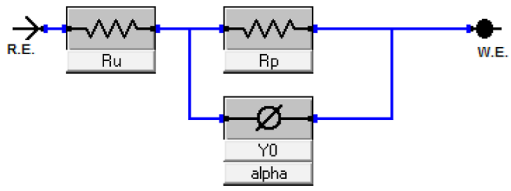

Figure 12. Equivalent circuit utilized in appropriating EIS outcomes. R_u: solution resistance, R_p: polarization resistance for uninhibited and inhibited solutions. R_p corresponds to charge-transfer resistance (R_{ct}), and R_f indicates inhibitive film resistance ($R_p = R_{ct} + R_f$).[43]

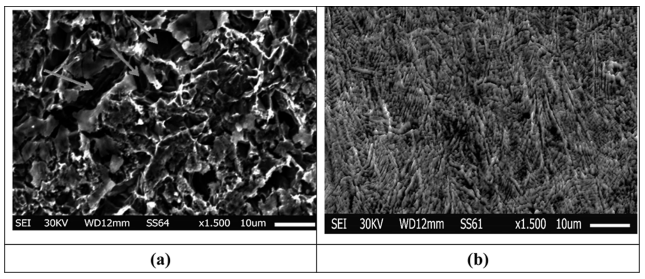

Figure 13. (a,b) SEM micrographs for CS-N80 after exposure to 1 M HCl for 1 day (a) and in the existence of 150 ppm of PIE (b).

Van't Hoff equation was used to compute the enthalpy of adsorption (ΔH_{ads}°)[40]

$$\log K_{ads} = \Delta H_{ads}^{\circ}/2.303RT + \text{constant} \quad (9)$$

Figure 8 displays the drawing of $\log K_{ads}$ with $1/T$ for CS-N80 in 1 M HCl with PIE. The entropy of adsorption (ΔS_{ads}°) can be computed by using the following formula

$$\Delta S_{ads}^{\circ} = (\Delta H_{ads}^{\circ} - \Delta G_{ads}^{\circ})/T \quad (10)$$

Table 4 provides a list of calculated values for ΔH_{ads}° and ΔS_{ads}°. The extract adsorption process is endothermic, as indicated by the positive value of ΔH_{ads}°. Literature pointed out that an exothermic process denotes either physisorption or chemisorption, whereas endothermic activity is connected with chemisorption.[41] The measured ΔH_{ads}° of 59.1 kJ mol^{-1} supports the possibility of chemical adsorption. Positive values of ΔS_{ads}° coincide with the adsorption of inhibitor compounds. An ordered layer is created on the adsorbed molecules at the solid/liquid interface.

3.3. Electrochemical Techniques. *3.3.1. Potentiodynamic Polarization.* Figure 9 demonstrates the cathodic and anodic curves attained using PP inspection at 298 K without PIE and in varying PIE concentrations for CS-N80 in 1 M HCl. It is demonstrated from Figure 9 that the anodic and cathodic plots were moved to more positive and negative values, respectively, suggesting that the extract may have a mixed inhibitory effect. Polarization data are produced from the PP measurement and utilized to examine the adsorption mechanism. The E_{corr} and i_{corr} values were determined by extrapolation findings from the polarization curve. The CR is computed using these parameters. The results of electrochemical parameters at altered PIE doses are recorded in Table 5. The addition of 150 ppm produced the best inhibitory efficiency value of 91.4% (Table 5). Table 5 contains the corrosion coefficients from the PP measurements like E_{corr}, i_{corr}, cathodic, and anodic (β_c and β_a) slopes, CR, θ, and % IE. Additionally, in comparison to the uninhibited sample, PIE lowered the CS-N80 oxidation and postponed hydrogen ion reduction on the cathode's surface without changing the techniques of these processes. In general, whenever the E_{corr} value is higher than 85 mV against the blank sample, the inhibitor is assorted as cathodic or anodic, while at shifts lower than ±85 mV, it is assorted as mixed type. Table 5 shows that the addition of PIE caused a change in the E_{corr} value lower than 85 mV, demonstrating an inhibition of mixed types. The adsorption mechanism was examined using the PP measurement findings. The anodic (β_a) and cathodic (β_c) Tafel slope values are essentially unchanged (almost parallel collection of cathodic and anodic lines), indicating that the inhibition mechanism remained unchanged.[42] The experimental data obtained via the WL technique and the Tafel curve findings are in good agreement.

3.3.2. Electrochemical Impedance Spectroscopy. EIS investigation graphs were utilized to demonstrate the corrosion behavior that was earlier indicated and also provide details about the kinetic activities and surface properties of the electrode. Figures 10 and11 show the Nyquist graph and Bode for CS-N80 in 1 M HCl without and with several doses of PIE at 25 °C, respectively. Figure 12 depicts the circuit employed to appropriate the values from EIS, where R_s is the solution resistance. This circuit provides a range of heterogeneity for corrosion electrodes by utilizing stationary phase elements (CPE) in place of capacitors. Table 6 shows that R_p values increase as the inhibitor concentration increases. The R_p value varies between 56.9 and 78.9 Ω/cm^2. This could imply that the inhibitor develops a protective coating on the electrode surface at all concentrations. The diameter of the semicircle in the Nyquist bends (Figure 10) progressively increased as the PIE concentration increased, suggesting that the charge-transfer process primarily regulates CS-N80 corrosion. Bode graphs (Figure 11) show that phase angles of the CS-N80 electrode were obtained at various concentrations of PIE and that impedance at low frequency increases with increasing extract content. These findings point to enhanced protective action for high concentrations of PIE because it adsorbs the surface of CS-N80 and blocks its energetic sites. The semicircular Nyquist plot form (Figure 10)[43] indicates the roughness and inhomogeneity properties of the electrode surface. Furthermore, the semicircle

Table 6. EIS Results without PIE and in Varying PIE Concentrations for CS-N80 in 1 M HCl at 298

conc., ppm	Y_0 (μ Ω^{-1} sn cm^{-2}) × 10^{-6}	n	Rp, Ω cm^2	Cdl, μF cm^{-2}	θ	% IE	χ^2
0	459	0.956	9.1 ± 0.1453	182 ± 0.1475			15.68×10^{-3}
25	257	0.960	56.9 ± 0.1764	128 ± 0.1551	0.840	84.0	20.91×10^{-3}
50	198	0.948	60.1 ± 0.1214	89 ± 0.1234	0.849	84.9	22.05×10^{-3}
75	175	0.941	73.2 ± 0.1321	76 ± 0.1325	0.876	87.6	19.19×10^{-3}
100	145	0.938	78.9 ± 0.1748	61 ± 0.1219	0.885	88.5	17.24×10^{-3}
125	129	0.929	85.1 ± 0.1457	50 ± 0.1412	0.893	89.3	20.42×10^{-3}
150	118	0.910	99.3 ± 0.1954	41 ± 0.1124	0.908	90.8	17.84×10^{-3}

https://doi.org/10.1021/acsomega.4c07543
ACS Omega 2024, 9, 44697−44713

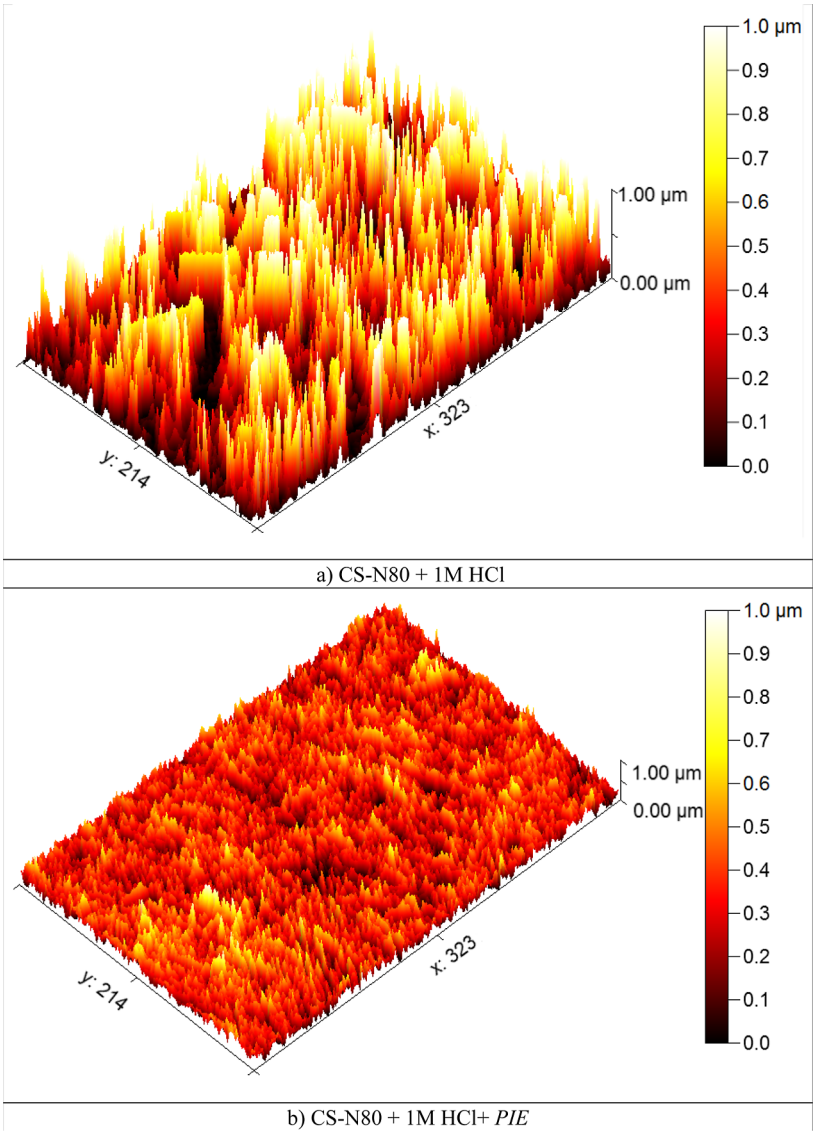

Figure 14. Effect of PIE inhibitor on CS-N80 surface morphology (AFM): (a) 1.0 M HCl (24 h) and (b) 1.0 M HCl + 150 ppm PIE (24 h, 25 °C).

Table 7. Surface Roughness Parameter Was Determined Based on AFM Measurement in 1 M HCl Solution Only and in the Presence of the Optimal Concentration of PIE at 150 ppm for 24 h at 25 °C

CS-N80 coupons	average roughness (*Ra*) nm	root mean square roughness (R_q) nm
CS-N80 in 1 M HCl (blank)	675	696
CS-N80 in 1 M HCl containing PIE	107	178

at the top of the frequency area is related to the time constant, which is also connected to the CPE (Y_o is its magnitude), which is considered a surface irregularity of the electrode and R_p. The values of Y_0 decrease as C_{dl} by raising the PIE concentrations. The impedance of a CPE is explained by eq 11[44]

$$Z_{CPE} = \frac{1}{Y_0(j\omega)^n} \tag{11}$$

where "Y_0" denotes the amount of CPE, "ω" denotes the frequency of the angular motion of the imaginary component's

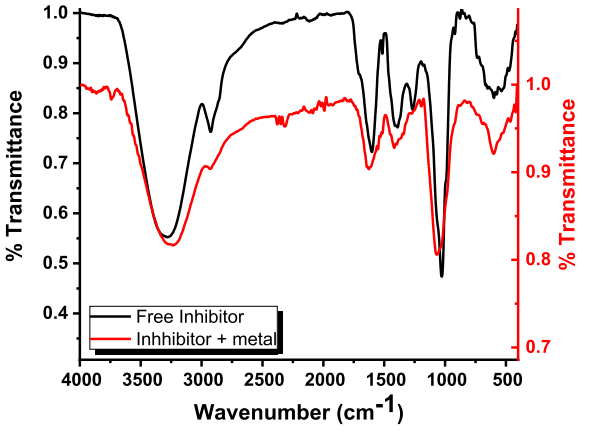

Figure 15. FT-IR spectrum of PIE and the extract adsorbed on the CS-N80 surface.

utmost impedance, "*j*" denotes the imaginative root, and "*n*" is a parameter that specifies the perversion of CPE which is a perfect capacitor when *n* equals 1. Due to the electrode roughness, dielectric constant, and heterogeneity of the metal surface, the *n*

https://doi.org/10.1021/acsomega.4c07543
ACS Omega 2024, 9, 44697−44713

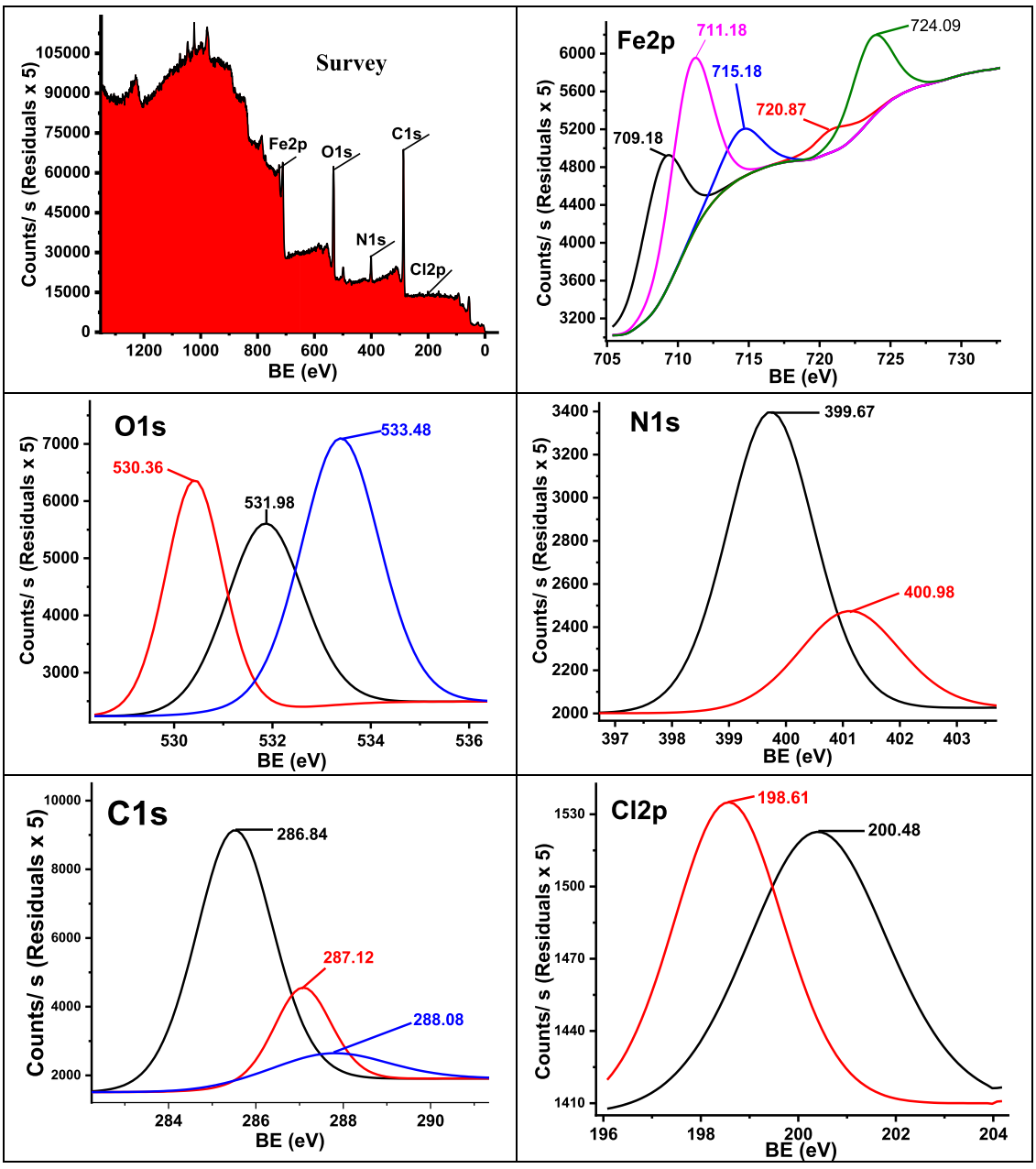

Figure 16. Photoelectric X-ray results from the survey, Fe 2p, O 1s, N 1s, C 1s, and Cl 2p for CS-N80 at 1 M HCl solution.

values range from 0 to 1. Here, data fitting was done using a CPE because the resulting (n) values (Table 6) fell inside the domain of 0.910−0.960. As is evident from Table 6, increasing the concentration of PIE causes a drop in Y_0 (CPE) relative to that of the blank solution. It results from the lowering of the native dielectric constant and/or the thickening of the layer of double electrical which is referred to as the Sumac molecule adsorption in the interface of CS-N80/solution. The quality of the circuit fitting was evaluated using the chi-square ($\chi 2$) value.[45] Table 6 shows that the obtained values of $\chi 2$ are between 15.68×10^{-3} and 22.06×10^{-3}, indicating a correct coincidence to the proposed circuit and a strong agreement between the fitted and experimental data. The evolution of a layer of adsorbed PIE on the CS-N80 surface causes an increase in % IE. Moreover, the capacitance and double-layer thickness decrease as C_{inh} rises.[46,47] The creation of the adsorbed layer from additives on the CS-N80 surface causes the % IE to grow; this layer increases and thickens as the concentration of the additives increases.[48]

3.4. Surface Examination. *3.4.1. Scanning Electron Microscopy.* In order to confirm the adsorption of PIE molecules on the CS-N80 surface, SEM analyses were performed. Figure 13 illustrates the morphological variations between the two conditions: CS was placed in 1 M HCl without the extract (Figure 13a), and CS-N80 was placed in 1 M HCl with 150 ppm of the extract (Figure 13b). In the acidic corrosive medium without PIE, the CS-N80 surface exhibits extensive corrosion. According to the CS-N80 surface morphology in the existence of PIE, the surface was smoother and pit-free. This is due to the PIE molecules adsorbing onto the surface and forming a preventive film that is irregularly distributed at the CS-N80 surface, reducing the interaction of CS-N80 with the corrosive solution due to adsorption of the PIE molecules on the CS surface, preventing it from corrosion.[49]

https://doi.org/10.1021/acsomega.4c07543
ACS Omega 2024, 9, 44697−44713

Table 8. BE, eV, for the Large Core Lines Observed for the Surface of CS-N80 Handled by PIE

	PIE	
core element	BE, eV	assignments
O 1s	530.36	Fe_2O_3
	531.98	$Fe(OH)_3$
	533.48	−OH−
C 1s	286.84	C−C, C−H,
	287.12	C═N,
	288.08	C═O
Fe 2p	709.18	Fe_2O_3/$Fe3O_4$/FeOOH $FeCl_3$
	711.18	
	715.18	
	720.87	
	724.09	
Cl 2p	198.61	Cl $2p^{3/2}$
	200.48	
N 1s	399.67	Fe-N_x (=N-structure)
	400.98	

3.4.2. Atomic Force Microscopy. AFM is indeed an excellent tool for obtaining precise measurements of the surface roughness. Figure 14a,b displays AFM images of the CS-N80 alloy surface, both without and with PIE. These images reveal surface characteristics quantified by R_a (average roughness) and R_q (root-mean-square roughness). Table 7 displays these roughness values for the altered conditions. The untreated sample exposed to a severe 1.0 M HCl solution suffered significant corrosion damage, as shown in Figure 14a. This resulted in a high average roughness of 675 nm. On the other hand, the existence of PIE in Figure 14b demonstrably smoothened the surface, reducing the average roughness by 107 nm. This significant improvement in smoothness indicates successful inhibitor adsorption onto the CS-N80 alloy. This strongly suggests the formation of a protective PIE film on the CS-N80 surface.[50]

3.4.3. FT-IR Spectroscopy. Figure 15 signifies the ATR-IR spectrum of PIE and the construction of the adsorbed film over the CS-N80 surface.[51] The FT-IR spectra of PIE, both before and after their adsorption on the CS-N80 surface, are shown in Figure 15. Based on the FT-IR spectra of PIE, the broad band at 3272 cm^{-1} can be classified as O−H, C−H, and N−H, and the broad band at (2927) cm^{-1} is related to stretching (C−H); the band at 1255 cm^{-1} is associated with C═O, C−O acid, and the band at 1032 cm^{-1} is associated with C−O. It can be seen from Figure 15 that there is a change in frequencies between the spectra of PIE and the corrosion product after CS-N80 is submerged, suggesting that PIE interacts with the CS-N80 surface through the functional groups of the extract.

3.4.4. X-ray Photoelectron Spectroscopy. The XPS examination provided detailed insights into the chemical composition at the interface between the CS-N80 surface and the plant extracts. Spectra were obtained from CS-N80 surfaces soaked in 1.0 M HCl solution with and without 150 ppm of the investigated PIE inhibitor for 24 h. High-resolution XPS spectroscopy became essential in both qualitative and quantitative analyses of the identified species at the metal/inhibitor interaction. Figure 16, shows XPS results from the survey, Fe 2p, O 1s, N 1s, C 1s, and Cl 2p at 1 M hydrochloric acid solution only and with 150 ppm of plant extract (Table 8). The XPS spectra of Fe 2p split into five peaks attributed to metallic iron, Fe_2O_3, and $Fe(OH)_3$ Fe 2p1/2 via Fe_3O_4, α-Fe_2O_3, and FeOOH. In studying the XPS spectra of C 1s, we establish three peaks attributed to C−C, C−O, and C═O.[52] Looking at the O 1s spectrum refers to metal oxide and O−H. Studying N 1s peaks attributed to N in the plant extract assesses the adsorption of PIE inhibitor strongly at the CS-N80 surface, as well as the two peaks of Cl 2p indicate the interaction of chloride anions with the substrate. The results of the XPS analysis confirm the adsorption of the PIE on the CS-N80 surface in 1 M HCl.

3.5. Theoretical Chemical Calculation. *3.5.1. Quantum Chemical Calculation (HOMO−LUMO).* Figure 17 shows the LUMO and HOMO orbitals for the major constituents of PIE with oleamide, palmitic acid, and 3-hydroxydodecanoic acid compounds. Table 9 demonstrates the E_{LUMO}, E_{HOMO}, dipole moment (μ), and energy gap (ΔE) for PIE constituents.

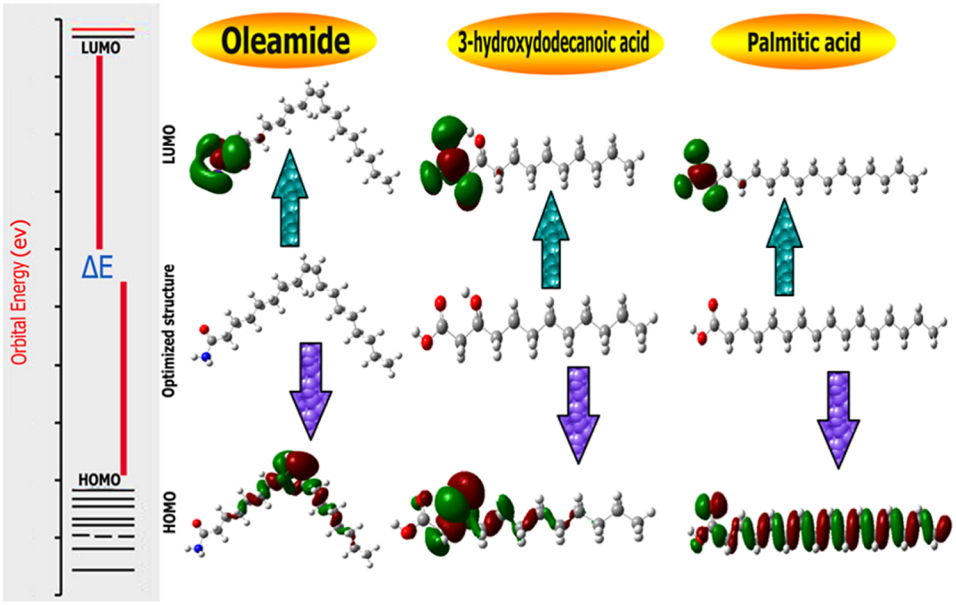

Figure 17. HOMO and LUMO orbitals for major three PIE compounds.

https://doi.org/10.1021/acsomega.4c07543
ACS Omega 2024, 9, 44697−44713

Table 9. Quantum Analysis of the Main Ingredients in PIE

parameters (variable)	oleamide	3-hydroxydodecanoic acid	palmitic acid
E_{HOMO} (eV)	−6.36	−7.40	−7.75
E_{LUMO}(eV)	−0.50	−0.52	−0.12
ΔE, (eV)($E_L - E_H$)	5.86	6.88	7.63
E_A (eV)	6.36	7.40	7.75
I_p (eV)	0.50	0.52	0.12
(eV)χ(electronegativity)	3.43	3.96	3.93
M	−3.43	−3.96	−3.93
η, eV	2.93	3.44	3.82
σ, eV	0.34	0.29	0.26
ω, eV	2.01	2.28	2.03
$\Delta E_{back\text{-}donation}$	−0.733	−0.860	−0.955
dipole moment (debye)	3.544	2.258	1.568
molecular surface area, Å^2	402.34	288.87	205.41

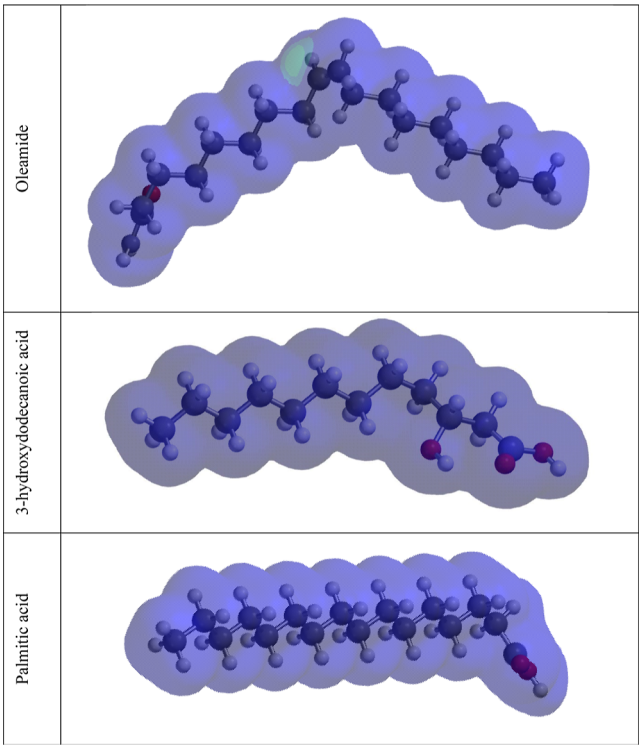

Figure 18. MEP surface of PIE.

The adsorption capacity of inhibitor molecules on the metal surface increases with a greater E_{HOMO} value and a decreased E_{LUMO} value, thereby enhancing corrosion IE. The energy gap (ΔE), defined as the difference between HOMO energy and LUMO energy, is a crucial parameter. According to its lower energy gap (ΔE) values, the examined PIE inhibitor is highly reactive, which results in a higher inhibitor efficiency form.[53] Furthermore, the ability of an inhibitor molecule to protect metal surfaces from corrosive conditions is significantly influenced by its molecular surface area. The inhibitory efficiency increases with larger molecular structures because the inhibitor molecules on CS-N80 cover a greater surface area. As a result, Table 9 illustrates that the compounds exhibiting the highest molecular surface area (oleamide, 3-hydroxydodecanoic acid, and palmitic acid) also have the highest inhibition proficiency. Therefore, constituents of PIE have the maximum adsorption tendency on the surface of CS-N80 as shown in Table 9 and Figure 17.

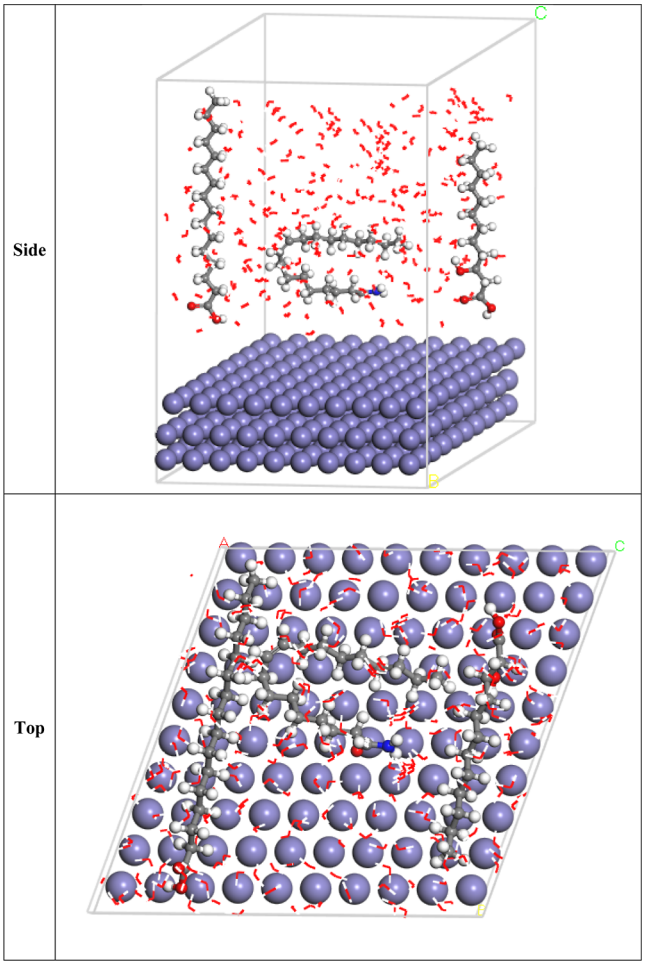

Figure 19. Most appropriate configuration for adsorption of three main molecules (PIE) on CS-N80 (final equilibrium configurations) on the iron (110) surface achieved by the adsorption locator module.

$$I_p(\text{ionization potential}) = -E_{HOMO} \quad (12)$$

$$(\text{electron affinity}) = -E_{LUMO} \quad (13)$$

$$\chi(\text{electronegativity}) = \frac{-(E_{LUMO} + E_{HOMO})}{2} \quad (14)$$

$$\mu(\text{potential}) = -\chi = \frac{(E_{LUMO} + E_{HOMO})}{2} \quad (15)$$

https://doi.org/10.1021/acsomega.4c07543
ACS Omega 2024, 9, 44697−44713

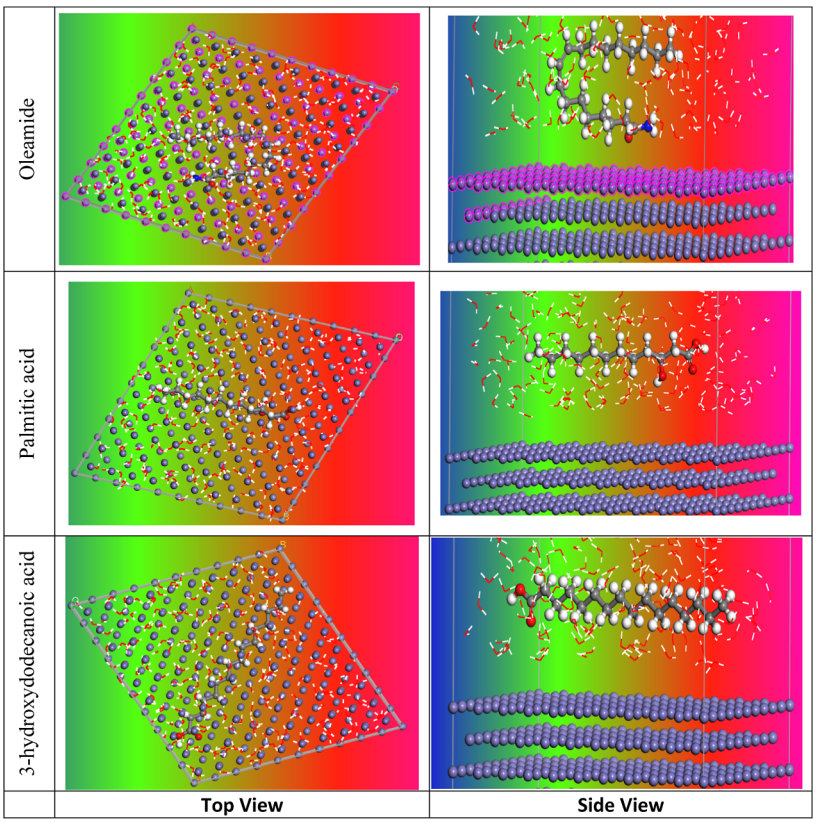

Figure 20. MC side and top views of the ideal configuration for the adsorption of PIE on Fe(110) surface.

Table 10. MC Parameters for Adsorption of PIE on Fe(110)

structures	total energy	adsorption energy, kcal mol^{-1}	rigid adsorption energy, kcal mol^{-1}	deformation energy, kcal mol^{-1}	compound dE_{ads}/dN, kcal mol^{-1}	H_2O dE_{ads}/dNi, kcal mol^{-1}
Fe (1 1 0) oleamide/H_2O	−311.513	−4661.857	−329.968	−4331.888	−1074.529	−18.28
Fe (1 1 0) 3-hydroxydodecanoic acid/H_2O	−312.606	−3722.942	−326.135	−3396.788	−132.765	−18.25
Fe (1 1 0) palmitic acid/H_2O	−41.584	−3478.343	−53.725	−3424.618	−138.0433	−16.49

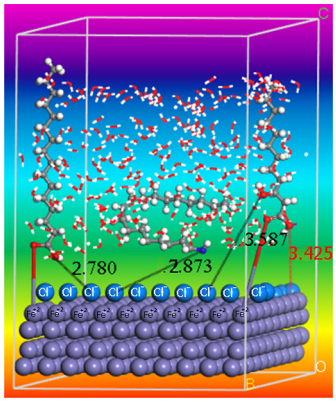

Figure 21. Mechanism of inhibition and radial distribution function of PIE on the Fe(110) surface in solution.

$$\eta(\text{hardness}) = \frac{(E_{\text{LUMO}} - E_{\text{HOMO}})}{2} \tag{16}$$

The definition of softness is the global hardness inverse, which is as follows

$$\sigma(\text{softness}) = 1/\eta \tag{17}$$

$$\omega(\text{electrophilicity index}) = \frac{\mu^2}{2\eta} \tag{18}$$

$$\Delta E_{\text{back donation}} = -\frac{\eta}{4} \tag{19}$$

The exchange of ΔN occurred between the metallic surface and the inhibitor

$$\Delta N(\text{fraction of electrons}) = \frac{(\chi_{\text{Fe}} - \chi_{\text{inh}})}{2(\eta_{\text{Fe}} + \eta_{\text{inh}})} \tag{20}$$

Since they are softer than neutral metallic, theoretical values of $\chi_{\text{Fe}} \approx 7$ eV and $\eta_{\text{Fe}} = 0$ are assumed based on the idea that $I = A$ for a bulk metal.

3.5.2. Molecular Electrostatic Potential Map. The molecular electrostatic potential (MEP) is a trustworthy diagnostic tool for hydrogen bond, electrophile, and nucleophile interaction sites. The MEP profile of the inhibitor utilized in this study is displayed in Figure 18. The region has high electron density and very negative MEP (nucleophilic interaction) and the highest positive zone, on the other hand (electrophilic attraction).[54]

3.5.3. MC Simulation. Figure 19 displays the highest proper adsorption arrangement for the PIE molecules (final equilibrium configurations). Figure 20 (left and right panels) illustrates this

https://doi.org/10.1021/acsomega.4c07543
ACS Omega 2024, 9, 44697−44713

Table 11. Comparison of Corrosion IE (% IE) of PIE with Other Plant Extracts

plant name	conc	metal/electrolyte	IE %	refs
Brahmi(Bacopa monnieri)	2 g/L	low carbon steel/0.5 M NaOH	80	61
Spondias cytherea	500 mg/L	mild steel/5 M H_2SO_4	67.72	62
Dioscorea septemloba	2 g/L	carbon steel/1 M HCl	72	63
Chamaerops humilis fruit	1.0 g/L	mild steel/1 M HCl	80.0	64
Euphorbia heterophylla llinneo	2 g/L	mild steel/1.5 M HCl	69	65
mint apple (Mentha rotundifolia)	2 mL/L	carbon steel/1 M HCl	87.0	66
Luffa cylindrica extract	1 g/L	MS in 0.5 M HCl	76	67
PIE	150 ppm	CS-N80/1.0 M HCl	92.1	Our results

position in both top and side viewpoints. By expanding the contact surface area among the inhibitor and Fe, this structure enhanced the inhibitor's inhibitory activity, which is useful for larger molecules. Table 10 shows the total energy, adsorption energy, and deformation energy obtained from the MC simulation. The total of the PIE molecule's internal and adsorption energies is known as its gross energy.[55] The various parameters obtained from the MC simulation are listed in Table 10. The total energy of the substrate−adsorbate contact, expressed in kilocalories per mole (kcal mol^{-1}), makes up the parameters. Adsorption energy is the total of the deformation and rigid energies added together. The adsorption energy, expressed in kcal mol^{-1}, is the energy released or used during adsorption of the relaxed adsorbate component onto the substrate surface. It is used to find centers of adsorption which have lowest energy on iron surfaces. For surface adsorption, it leads to a protective thin organic layer that decreases the CR of the metal. The table displays higher adsorption energies (−4661.857, −3722.942, and −3478.343 kcal mol^{-1} for oleamide, 3-hydroxydodecanoic acid, and palmitic acid compounds, respectively). The output shows that the three compounds are highly efficient adsorptive inhibitors.

The energy of the rigid adsorption, on the other hand, provides the energy, expressed as kcal mol^{-1}, that is released (or needed) when the components of the unrelaxed adsorbate are adsorbed on the substrate, that is, before the geometry optimization process. Additionally, the energy released when the adsorbed components of the adsorbate relax on the surface of the substrate is referred to as the deformation energy, measured kcal mol^{-1}.[56] The simulation findings in Table 10 confirm that the tested PIE adsorbs at a high rate on the CS-N80 surface.

3.6. Mechanism of Corrosion Inhibition in Acidic Media. The research on the adsorption of inhibitors onto the surface of the metal has found that the efficiency of an inhibitor may be determined by quantifying the amount of extract adsorbed on the metal's surface. This development can be manifested in the form of a reduction in the rate at which the metal corrodes. According to Shreir et al., the adsorbed inhibitors can be directly measured using solution depletion and radiotracer detection techniques. The adsorption behavior of an inhibitor stipulates that corrosion may be prevented within the region of the metal's surface that is already inundated with the adsorbed inhibitive materials. In essence, the level of inhibition is commensurate with the fraction of the metal surface that is covered by the adsorbed inhibitor.[57]

The PIE plant mainly consisted oleamide, palmitic acid, and 3-hydroxydodecanoic acid compounds. The constituents of plant extracts can be found as neutral molecules or cations (protonated species) in aqueous acidic solutions. Two adsorption modes might generally be taken into consideration (Figure 21). Through the chemisorption method, which involves displacing water molecules off the metal surface and exchanging electrons between the N and O atoms and the metal surface, the neutral species may adsorb on a metal surface, causing the formation of a coordinate-type bond.[58] Physical adsorption arises when PIE molecules are instantly protonated in an HCl solution to create a positive charge species. It is believed that the Fe surface at E_{corr} in HCl is positively charged. The surface therefore acquires a negative charge due to the adsorption of Cl^- anions from the HCl solution. Electrostatic interactions between positively charged molecules and a negatively charged CS-N80 surface cause the molecules in the extract to be physically adsorbed to the metal surface.[59] The bond length between the metal and PIE is estimated using the radial distribution function. The peak, which is connected to chemisorption in Figure 21, occurs from "1 Å up to 3.5 Å and represents the length of small bonds. Conversely, peaks larger than 3.5 Å are linked to physisorption.[60] Additionally, the PIE atom shows that inhibitors are chemisorbed on the iron surface because mostly the iron bond length is than 3.5 Å".

3.7. Comparison of % IE PIE with Different Plant Extracts. The corrosion hindrance ability of our PIE is compared with that of the previously reported extracts[61−67] and is presented in Table 11. It is evident that our PIE demonstrates a strong corrosion inhibition capability, with an efficiency of 92.1% at a concentration of 150 ppm. This efficiency was higher than that observed in other plant extracts, which varied from around 67 to 96.72%. Overall, our results demonstrate that PIE has a significant potential as a corrosion inhibitor.

4. CONCLUSIONS

The study investigated the inhibitory effect of PIE on the dissolution of CS-N80 in hydrochloric acid (HCl) solution in the range of 298−318 K at all concentrations. The experimental investigation involves electrochemical techniques, chemical techniques, and theoretical studies. The activation kinetic parameter values obtained from the experiments supported the adsorption of PIE at various temperatures on the CS-N80 surface. As the temperature rose, the PIE inhibitory effectiveness increased and reached 92.1%, indicating chemical adsorption. The positive ΔG_{ads} values indicate the spontaneity of PIE adsorbed on the CS-N80 surface and the stability of the adsorbed layer on the CS-N80 surface. The adsorption of PIE over the CS-N80 surface obeyed the Temkin adsorption isotherm. Analysis of PP data suggested that PIE acts as a mixed-type inhibitor. SEM equipped with an energy-dispersive system, XPS, and FT-IR were used to observe the micro-morphology, composition, and elemental chemical state of the different samples, respectively. DFT calculations are employed to provide a theoretical basis for the observed inhibitory

https://doi.org/10.1021/acsomega.4c07543
ACS Omega 2024, 9, 44697−44713

behavior of the substances under investigation. Additionally, the MC calculations show that there is a strong adsorptive interaction that takes place between the PIE inhibitor and the iron surface.

■ ASSOCIATED CONTENT

Data Availability Statement

The authors confirm that the data supporting the findings of this study are available within the article and/or its supporting file.

■ AUTHOR INFORMATION

Corresponding Author

Mariem M. Motawea − *Department of Chemistry, College of Science, University of Bisha, Bisha 61922, Saudi Arabia; Department of Basic Science, Delta Higher Institute for Engineering and Technology, Mansoura 35681, Egypt;* orcid.org/0000-0002-9472-7678; Email: dr_mmm_2018@yahoo.com

Authors

Abeer Y. H. Alamry − *Department of Chemistry, College of Science, University of Bisha, Bisha 61922, Saudi Arabia*

Nora S. Al-Subaie − *Department of Chemistry, College of Science, University of Bisha, Bisha 61922, Saudi Arabia*

Wafa S. Alshahrani − *Department of Chemistry, College of Science, University of Bisha, Bisha 61922, Saudi Arabia*

Mai M. A. H. Shanab − *Chemistry Department, College of Science and Humanities, Prince Sattam Bin Abdulaziz University, Al-kharj 11942, Saudi Arabia; Forensic and Toxicology Lab., Forensic Medicine, Mansoura 35511, Egypt*

Complete contact information is available at: https://pubs.acs.org/10.1021/acsomega.4c07543

Notes

The authors declare no competing financial interest.

■ ACKNOWLEDGMENTS

The authors are thankful to the Deanship of Graduate Studies and Scientific Research at the University of Bisha for supporting this work through the Fast-Track Research Support Program.

■ REFERENCES

(1) Chauhan, L. R.; Gunasekaran, G. Corrosion Inhibition of Mild Steel by Plant Extract in Dilute HCl Medium. *Corros. Sci.* **2007**, *49* (3), 1143−1161.

(2) Lalitha, A.; Ramesh, S.; Rajeswari, S. Surface Protection of Copper in Acid Medium by Azoles and Surfactants. *Electrochim. Acta* **2005**, *51* (1), 47−55.

(3) de Souza Morais, W. R.; da Silva, J. S.; Queiroz, N. M. P.; de Paiva e Silva Zanta, C. L.; Ribeiro, A. S.; Tonholo, J. Green Corrosion Inhibitors Based on Plant Extracts for Metals and Alloys in Corrosive Environment: A Technological and Scientific Prospection. *Appl. Sci.* **2023**, *13* (13), 7482.

(4) Quraishi, M. A.; Sardar, R. Aromatic Triazoles as Corrosion Inhibitors for Mild Steel in Acidic Environments. *Corrosion* **2002**, *58* (9), 748−755.

(5) Ahmed E S, J.; Ganesh, G. M. A Comprehensive Overview on Corrosion in RCC and Its Prevention Using Various Green Corrosion Inhibitors. *Buildings* **2022**, *12* (10), 1682.

(6) Tamalmani, K.; Husin, H. Review on Corrosion Inhibitors for Oil and Gas Corrosion Issues. *Appl. Sci.* **2020**, *10* (10), 3389.

(7) Zakeri, A.; Bahmani, E.; Aghdam, A. S. R. Plant Extracts as Sustainable and Green Corrosion Inhibitors for Protection of Ferrous Metals in Corrosive Media: A Mini Review. *Corros. Commun.* **2022**, *5*, 25−38.

(8) Li, H.-J.; Zhang, W.; Wu, Y.-C. Anti-Corrosive Properties of Alkaloids on Metals. In *Alkaloids-Their Importance in Nature and Human Life*; IntechOpen, 2018.

(9) Elgyar, O. A.; Ouf, A. M.; El-Hossiany, A.; Fouda, A. S. The Inhibition Action of Viscum Album Extract on the Corrosion of Carbon Steel in Hydrochloric Acid Solution. *Biointerface Res. Appl. Chem.* **2021**, *11* (6), 14344−14358.

(10) Fouda, A. S.; El-Gharkawy, E.-S.; Ramadan, H.; El-Hossiany, A. Corrosion Resistance of Mild Steel in Hydrochloric Acid Solutions by Clinopodium Acinos as a Green Inhibitor. *Biointerface Res. Appl. Chem.* **2021**, *11* (2), 9786−9803.

(11) Fouda, A. S.; Azeem, M. A.; Mohamed, S. A.; El-Hossiany, A.; El-Desouky, E. Corrosion Inhibition and Adsorption Behavior of Nerium Oleander Extract on Carbon Steel in Hydrochloric Acid Solution. *Int. J. Electrochem. Sci.* **2019**, *14* (4), 3932−3948.

(12) Ezzat, A.; Motaal, S. M. A.; Ahmed, A. S.; Sallam, H. B.; El-Hossiany, A.; Fouda, A. Corrosion Inhibition of Carbon Steel in 2.0 M HCl Solution Using Novel Extract (Pulicaria Undulate). *Biointerface Res. Appl. Chem.* **2022**, *12* (5), 6415−6427.

(13) Fouda, A. E. S.; Motaal, S. M. A.; Ahmed, A. S.; Sallam, H. B.; Ezzat, A.; El-Hossiany, A. Corrosion Protection of Carbon Steel in 2M HCl Using Aizoon Canariense Extract. *Biointerface Res. Appl. Chem.* **2021**, *12* (1), 230−243.

(14) Xu, N.; Yang, X. B.; Zhang, Q. H. Insight into Interfacial Adsorption and Inhibition Mechanism of Aconitum Carmichaelii Debx Extract as High-Efficient Corrosion Inhibitor for Carbon Steel in Acidic Solution. *J. Mol. Liq.* **2024**, *393*, 123602.

(15) Emmanuel, A. C.; Udeokpote, G. C. Ethanol Extract of Vernonia Amygdalina Leaf as a Green Corrosion Inhibitor for Carbon Steel in Solution of HCl. *Commun. Phys. Sci.* **2023**, *10* (3), 182−193.

(16) Almahdy, M. S.; Molouk, A. F.; El-Hossiany, A.; Fouda, A. E. Electrochemical Studies of Erica Arborea Extract as a Green Corrosion Inhibitor for C-Steel in Sulfuric Acid Medium. *Biointerface Res. Appl. Chem.* **2023**, *13* (5), 472.

(17) Verma, C.; Chauhan, D. S.; Aslam, R.; Banerjee, P.; Aslam, J.; Quadri, T. W.; Zehra, S.; Verma, D. K.; Quraishi, M. A.; Dubey, S.; et al. Principles and Theories of Green Chemistry for Corrosion Science and Engineering: Design and Application. *Green Chem.* **2024**, *26* (8), 4270−4357.

(18) Wang, Q.; Wu, X.; Zheng, H.; Liu, L.; Zhang, Q.; Zhang, A.; Yan, Z.; Sun, Y.; Li, Z.; Li, X. Evaluation for Fatsia Japonica Leaves Extract (FJLE) as Green Corrosion Inhibitor for Carbon Steel in Simulated Concrete Pore Solutions. *J. Build. Eng.* **2023**, *63*, 105568.

(19) Kamal, C.; Sethuraman, M. G. Caulerpin— A Bis-Indole Alkaloid as a Green Inhibitor for the Corrosion of Mild Steel in 1 M HCl Solution from the Marine Alga Caulerpa Racemosa. *Ind. Eng. Chem. Res.* **2012**, *51* (31), 10399−10407.

(20) Abdel-Gaber, A. M.; Abd-El-Nabey, B. A.; Saadawy, M. The Role of Acid Anion on the Inhibition of the Acidic Corrosion of Steel by Lupine Extract. *Corros. Sci.* **2009**, *51* (5), 1038−1042.

(21) Oguzie, E. E.; Onuchukwu, A. I.; Okafor, P. C.; Ebenso, E. E. Corrosion Inhibition and Adsorption Behaviour of Ocimum Basilicum Extract on Aluminium. *Pigm. Resin Technol.* **2006**, *35* (2), 63−70.

(22) Gokhale, S., Ellis, S. API Specification 5CT N-80 Grade Casing May Burst or Part Unexpectedly If Supplementary Metallurgical Requirements Are Not Specified. *SPE/IADC Drilling Conference and Exhibition* 2005, SPE, SPE−92431.

(23) Shabani-Nooshabadi, M.; Ghandchi, M.-S. Introducing the Santolina Chamaecyparissus Extract as a Suitable Green Inhibitor for 304 Stainless Steel Corrosion in Strong Acidic Medium. *Metall. Mater. Trans. A* **2015**, *46*, 5139−5148.

(24) Zeino, A.; Abdulazeez, I.; Khaled, M.; Jawich, M. W.; Obot, I. B. Mechanistic Study of Polyaspartic Acid (PASP) as Eco-Friendly Corrosion Inhibitor on Mild Steel in 3% NaCl Aerated Solution. *J. Mol. Liq.* **2018**, *250*, 50−62.

(25) Abdel-Rehim, S. S.; Khaled, K. F.; Abd-Elshafi, N. S. Electrochemical Frequency Modulation as a New Technique for Monitoring Corrosion Inhibition of Iron in Acid Media by New Thiourea Derivative. *Electrochim. Acta* **2006**, *51* (16), 3269−3277.

(26) Olasunkanmi, L. O.; Ebenso, E. E. Experimental and Computational Studies on Propanone Derivatives of Quinoxalin-6-Yl-4, 5-Dihydropyrazole as Inhibitors of Mild Steel Corrosion in Hydrochloric Acid. *J. Colloid Interface Sci.* **2020**, *561*, 104−116.
(27) Eno, E. A.; Mbonu, J. I.; Louis, H.; Patrick-Inezi, F. S.; Gber, T. E.; Unimuke, T. O.; Okon, E. E.; Benjamin, I.; Offiong, O. E. Antimicrobial activities of 1-phenyl-3-methyl-4-trichloroacetyl-pyrazolone: Experimental, DFT studies, and molecular docking investigation. *J. Indian Chem. Soc.* **2022**, *99* (7), 100524.
(28) Becke, A. D. Density-functional thermochemistry. I. The effect of the exchange-only gradient correction. *J. Chem. Phys.* **1992**, *96* (3), 2155−2160.
(29) Stephens, P. J.; Devlin, F. J.; Chabalowski, C. F.; Frisch, M. J. Ab initio calculation of vibrational absorption and circular dichroism spectra using density functional force fields. *J. Phys. Chem. A* **1994**, *98* (45), 11623−11627.
(30) Ansari, K. R.; Quraishi, M. A. Experimental and Quantum Chemical Evaluation of Schiff Bases of Isatin as a New and Green Corrosion Inhibitors for Mild Steel in 20% H2SO4. *J. Taiwan Inst. Chem. Eng.* **2015**, *54*, 145−154.
(31) Khaled, M. A.; Ismail, M. A.; El-Hossiany, A. A.; Fouda, A. E.-A. S. Novel Pyrimidine-Bichalcophene Derivatives as Corrosion Inhibitors for Copper in 1 M Nitric Acid Solution. *RSC Adv.* **2021**, *11* (41), 25314−25333.
(32) Etaiw, S. E. H.; Hassan, G. S.; El-Hossiany, A. A.; Fouda, A. S. Nano-Metal−Organic Frameworks as Corrosion Inhibitors for Strengthening Anti-Corrosion Behavior of Carbon Steel in a Sulfuric Acid Environment: From Synthesis to Applications. *RSC Adv.* **2023**, *13* (22), 15222−15235.
(33) Dkhireche, N.; Galai, M.; El Kacimi, Y.; Rbaa, M.; Ouakki, M.; Lakhrissi, B.; Touhami, M. E. New Quinoline Derivatives as Sulfuric Acid Inhibitor's for Mild Steel. *Anal. Bioanal. Electrochem.* **2018**, *9* (6), 111−135.
(34) Fouda, A. S.; Shalabi, K.; E-Hossiany, A. Moxifloxacin Antibiotic as Green Corrosion Inhibitor for Carbon Steel in 1 M HCl. *J. Bio-and Tribo-Corrosion* **2016**, *2*, 18.
(35) Jiang, L.; Qiang, Y.; Lei, Z.; Wang, J.; Qin, Z.; Xiang, B. Excellent Corrosion Inhibition Performance of Novel Quinoline Derivatives on Mild Steel in HCl Media: Experimental and Computational Investigations. *J. Mol. Liq.* **2018**, *255*, 53−63.
(36) Fouda, A. S.; El-Ghaffar, M. A. A.; Sherif, M. H.; El-Habab, A. T.; El-Hossiany, A. Novel Anionic 4-Tert-Octyl Phenol Ethoxylate Phosphate Surfactant as Corrosion Inhibitor for C-Steel in Acidic Media. *Prot. Met. Phys. Chem. Surfaces* **2020**, *56* (1), 189−201.
(37) Fouda, A. S.; El-Dossoki, F. I.; El-Hossiany, A.; Sello, E. A. Adsorption and Anticorrosion Behavior of Expired Meloxicam on Mild Steel in Hydrochloric Acid Solution. *Surf. Eng. Appl. Electrochem.* **2020**, *56* (4), 491−500.
(38) Hou, B. S.; Zhang, Q. H.; Li, Y. Y.; Zhu, G. Y.; Liu, H. F.; Zhang, G. A. A Pyrimidine Derivative as a High Efficiency Inhibitor for the Corrosion of Carbon Steel in Oilfield Produced Water under Supercritical CO2 Conditions. *Corros. Sci.* **2020**, *164*, 108334.
(39) Fouda, A. S.; El-Mekabaty, A.; Shaaban, I. E. I.; El-Hossiany, A. Synthesis and Biological Evaluation of Novel Thiophene Derivatives as Green Inhibitors for Aluminum Corrosion in Acidic Media. *Prot. Met. Phys. Chem. Surfaces* **2021**, *57* (5), 1060−1075.
(40) Abdallah, M.; Al-Abdali, F. H.; Kamar, E. M.; El-Sayed, R.; Abdel Hameed, R. Corrosion Inhibition of Aluminum in 1.0 M HCl Solution by Some Nonionic Surfactant Compounds Containing Five Membered Heterocyclic Moiety. *Chem. Data Collect.* **2020**, *28*, 100407.
(41) Fouda, A. S.; Etaiw, S. E. H.; Ibrahim, A. M.; El-Hossiany, A. A. Insights into the Use of Two Novel Supramolecular Compounds as Corrosion Inhibitors for Stainless Steel in a Chloride Environment: Experimental as Well as Theoretical Investigation. *RSC Adv.* **2023**, *13* (50), 35305−35320.
(42) Fouda, A. S.; Abdel-Wahed, H. M.; Atia, M. F.; El-Hossiany, A. Novel Porphyrin Derivatives as Corrosion Inhibitors for Stainless Steel 304 in Acidic Environment: Synthesis, Electrochemical and Quantum Calculation Studies. *Sci. Rep.* **2023**, *13* (1), 17593.
(43) Yıldız, R.; Arslanhan, S.; Döner, A.; Baran, M. F. Corrosion behavior of mild steel in 1 M HCl with Cyclotrichium niveum as a green inhibitor. *Mater. Chem. Phys.* **2024**, *312*, 128654.
(44) Yi, P.; Dong, C.; Xiao, K.; Man, C.; Li, X. In-situ investigation of the semiconductive properties and protective role of Cu_2O layer formed on copper in a borate buffer solution. *J. Electroanal. Chem.* **2018**, *809*, 52−58.
(45) Behpour, M.; Ghoreishi, S. M.; Mohammadi, N.; Soltani, N.; Salavati-Niasari, M. Investigation of Some Schiff Base Compounds Containing Disulfide Bond as HCl Corrosion Inhibitors for Mild Steel. *Corros. Sci.* **2010**, *52* (12), 4046−4057.
(46) Eissa, M.; Etaiw, S. H.; El-Waseef, E. E.; El-Hossiany, A.; Fouda, A. S. The Impact of Environmentally Friendly Supramolecular Coordination Polymers as Carbon Steel Corrosion Inhibitors in HCl Solution: Synthesis and Characterization. *Sci. Rep.* **2024**, *14* (1), 2413.
(47) Harrington, S. P.; Devine, T. M. Analysis of electrodes displaying frequency dispersion in Mott-Schottky tests. *J. Electrochem. Soc.* **2008**, *155*, C381−C386.
(48) Salleh, S. Z.; Yusoff, A. H.; Zakaria, S. K.; Taib, M. A. A.; Abu Seman, A.; Masri, M. N.; Mohamad, M.; Mamat, S.; Ahmad Sobri, S.; Ali, A.; et al. Plant Extracts as Green Corrosion Inhibitor for Ferrous Metal Alloys: A Review. *J. Clean. Prod.* **2021**, *304*, 127030.
(49) Ibrahim, M. B.; Sulaiman, Z.; Usman, B.; Ibrahim, M. A. Effect of Henna Leaves on the Corrosion Inhibition of Tin in Acidic and Alkaline Media. *World J. App. Chem.* **2019**, *4* (4), 45−51.
(50) Mahmoud, A. A.; Abdelfattah, M. O.; El-Hossiany, A.; Fouda, A. S. Eco-Friendly Approach to Corrosion Inhibition of Copper in HNO_3 Solution by the Expired Tylosin Drug. *Biointerface Res. Appl. Chem.* **2022**, *12* (4), 5116−5130.
(51) Fouda, A. S.; El-Maksoud, S. A.; El-Hossiany, A.; Ibrahim, A. Evolution of the Corrosion-Inhibiting Efficiency of Novel Hydrazine Derivatives against Corrosion of Stainless Steel 201 in Acidic Medium. *Int. J. Electrochem. Sci.* **2019**, *14* (7), 6045−6064.
(52) Fouda, A. E.; El-Dossoki, F.; Hamed, E.; El-Hossiany, A. Inhibition Efficiency of Erdosteine Drug for 304L Stainless Steel Corrosion and Its Solvation Thermodynamic Parameters. *Egypt. J. Chem.* **2022**, *65* (132), 455−475.
(53) Nkungli, N. K.; Ghogomu, J. N. Theoretical Analysis of the Binding of Iron (III) Protoporphyrin IX to 4-Methoxyacetophenone Thiosemicarbazone via DFT-D3, MEP, QTAIM, NCI, ELF, and LOL Studies. *J. Mol. Model.* **2017**, *23*, 200.
(54) Mumit, M. A.; Pal, T. K.; Alam, M. A.; Islam, M. A.-A.-A.-A.; Paul, S.; Sheikh, M. C. DFT Studies on Vibrational and Electronic Spectra, HOMO−LUMO, MEP, HOMA, NBO and Molecular Docking Analysis of Benzyl-3-N-(2, 4, 5-Trimethoxyphenylmethylene) Hydrazinecarbodithioate. *J. Mol. Struct.* **2020**, *1220*, 128715.
(55) Chkirate, K.; Azgaou, K.; Elmsellem, H.; El Ibrahimi, B.; Sebbar, N. K.; Anouar, E. H.; Benmessaoud, M.; El Hajjaji, S.; Essassi, E. M. Corrosion Inhibition Potential of 2-[(5-Methylpyrazol-3-Yl) Methyl] Benzimidazole against Carbon Steel Corrosion in 1 M HCl Solution: Combining Experimental and Theoretical Studies. *J. Mol. Liq.* **2021**, *321*, 114750.
(56) El-Asri, A.; Jmiai, A.; Bourzi, H.; Lin, Y.; El Issami, S. Chemistry of the Interaction between Imidazole Derivatives as Corrosion Inhibitors Molecules and Copper/Brass/Zinc Surfaces: A DFT, Reactive and Classical Molecular Force Fields Study. *Surf. Interfaces* **2024**, *44*, 103799.
(57) Burstein, G. T.; Shreir, L. L.; Jarman, R. A. *Corrosion-Vol. 2.: Corrosion Control*; Butterworth-Heinemann: Oxford, 2000.
(58) Palumbo, G.; Berent, K.; Proniewicz, E.; Banaś, J. Guar Gum as an Eco-Friendly Corrosion Inhibitor for Pure Aluminium in 1-M HCl Solution. *Materials* **2019**, *12* (16), 2620.
(59) Fouda, A. S.; Ibrahim, H.; Rashwaan, S.; El-Hossiany, A.; Ahmed, R. M. Expired Drug (Pantoprazole Sodium) as a Corrosion Inhibitor for High Carbon Steel in Hydrochloric Acid Solution. *Int. J. Electrochem. Sci.* **2018**, *13* (7), 6327−6346.
(60) Abdel-Azim, K.; Saleh, M.; Abdelshafi, N. S.; Khaled, K. F. Studies on the Effect of Some Pyrimidine Derivatives on the Corrosion

https://doi.org/10.1021/acsomega.4c07543
ACS Omega 2024, 9, 44697−44713

of Iron in 1M Hydrochloric Acid. *Egypt. J. Chem.* **2021**, *64* (7), 3475−3488.
(61) Al Hasan, N. H. J.; Alaradi, H. J.; Al Mansor, Z. A. K.; Al Shadood, A. H. J. The Dual Effect of Stem Extract of Brahmi (Bacopamonnieri) and Henna as a Green Corrosion Inhibitor for Low Carbon Steel in 0.5 M NaOH Solution. *Case Stud. Constr. Mater.* **2019**, *11*, No. e00300.
(62) Al-Sahlanee, H. H.; Sultan, A.-W. A.; Al-Faize, M. M. Corrosion Inhibition of Carbon Steel in 1M HCl Solution Using Sesbania Sesban Extract. *Aquat. Sci. Technol.* **2013**, *1* (2), 135−151.
(63) Emori, W.; Zhang, R.-H.; Okafor, P. C.; Zheng, X.-W.; He, T.; Wei, K.; Lin, X.-Z.; Cheng, C.-R. Adsorption and Corrosion Inhibition Performance of Multi-Phytoconstituents from Dioscorea Septemloba on Carbon Steel in Acidic Media: Characterization, Experimental and Theoretical Studies. *Colloids Surf., A* **2020**, *590*, 124534.
(64) Fekkar, G.; Yousfi, F.; Elmsellem, H.; Aiboudi, M.; Ramdani, M.; Abdel-Rahman, I.; Hammouti, B.; Bouyazza, L. Eco-Friendly Chamaerops Humilis L. Fruit Extract Corrosion Inhibitor for Mild Steel in 1 M HCl. *Int. J. Corros. Scale Inhib.* **2020**, *9* (2), 446−459.
(65) Akinbulumo, O. A.; Odejobi, O. J.; Odekanle, E. L. Thermodynamics and Adsorption Study of the Corrosion Inhibition of Mild Steel by Euphorbia Heterophylla L. Extract in 1.5 M HCl. *Results Mater.* **2020**, *5*, 100074.
(66) Khadraoui, A.; Khelifa, A.; Boutoumi, H.; Karzazi, Y.; Hammouti, B.; Al-Deyab, S. S. The Oil from Mentha Rotundifolia as Green Inhibitor of Carbon Steel Corrosion in Hydrochloric Acid. *Chem. Eng. Commun.* **2016**, *203* (2), 270−277.
(67) Ogunleye, O. O.; Arinkoola, A. O.; Eletta, O. A.; Agbede, O. O.; Osho, Y. A.; Morakinyo, A. F.; Hamed, J. O. Green Corrosion Inhibition and Adsorption Characteristics of Luffa Cylindrica Leaf Extract on Mild Steel in Hydrochloric Acid Environment. *Heliyon* **2020**, *6* (1), No. e03205.

https://doi.org/10.1021/acsomega.4c07543
ACS Omega 2024, 9, 44697−44713